Journal of Drug Delivery Science and Technology 110 (2025) 107070

Contents lists available at ScienceDirect

Journal of Drug Delivery Science and Technology

journal homepage: www.elsevier.com/locate/jddst

Exploring intranasal delivery of peptide and protein nanoparticles by a thermoresponsive hydrogel

Tanisha Tabassum Sayka Khan [a,b,c], Zara Sheikh [b,c], Ali Fathi [d,e], Simin Maleknia [e], Farshad Oveissi [d,e], Terence Abrams [e], Will Knox [e], Luca Casettari [f], Mattia Tiboni [f], Julie Suman [g], Hui Xin Ong [a,b,*], Daniela Traini [a,b,**]

[a] Macquarie Medical School, Faculty of Medicine, Health and Human Sciences, Macquarie University, Sydney, NSW 2109, Australia
[b] Respiratory Technology, Woolcock Institute of Medical Research, Sydney, NSW 2113, Australia
[c] School of Pharmacy, Brac University, Dhaka 1212, Bangladesh
[d] School of Chemical and Biomolecular Engineering, The University of Sydney, NSW 2006, Australia
[e] Tetratherix Technology Pty Ltd, Sydney, NSW 2015, Australia
[f] Department of Biomolecular Sciences, School of Pharmacy, University of Urbino Carlo Bo, Urbino 61029, Italy
[g] Aptar Pharma, Congers, NY 10920, USA

ARTICLE INFO

Keywords:
Bovine serum albumin
In situ gel
Microfluidic
Nanocarriers
Nasal drug delivery
PNPHO polymer

ABSTRACT

Effective delivery of peptide or protein-based drugs (PPDs) remains a challenge as parenteral routes are invasive and PPDs are subjected to enzymatic degradation via the oral route. As such, intranasal (IN) route is an effective, non-invasive approach for delivering PPDs locally, systemically, and to the central nervous system (CNS), while maintaining the stability of the drugs. The study investigates the potential of a novel thermoresponsive polymer (PNPHO), as a carrier to facilitate IN delivery of peptides/proteins. Two types of nanoparticle formulations (Low-F and High-F) using a low and a high PNPHO concentration (20 mg/mL and 35 mg/mL) were prepared with bovine serum albumin (BSA) incorporated in it. Both formulations exhibited good physicochemical properties in terms of particle size (Low-F: 29 nm; High-F: 39 nm), polydispersity index (PDI) (<0.3) and zeta (ζ) potential (−3 to −6 mV) with a high encapsulation efficiency (EE) (86 %–96 %) maintained at 4 °C during a 4-week stability study. High-F formulation demonstrated a significantly greater aerosol drug deposition in the entire nasal cavity and in the olfactory region *in vitro* compared to free BSA at 45° spray angle. Both formulations were found to be non-toxic when tested on nasal epithelial cell lines. Importantly, a significant increase in transepithelial resistance was observed for the nasal epithelial cells post 4 h treatment with High-F along with a significant reduction in BSA transport across the cells compared to free drug, indicating tightening of cellular junctions and prolonged drug residence time owing to its mucoadhesive property. Altogether, the findings suggest that PNPHO polymer is a potential carrier for targeted delivery of peptide/protein using the IN route.

1. Introduction

PPDs are conventionally administered via parenteral routes, which are invasive, painful, have a higher risk of systemic side effects due to lack of target specificity, and often lead to poor patient acceptability [1,2]. While oral route is generally preferred for better patient compliance, it is not suitable for peptide or protein delivery due to their high susceptibility to enzymatic degradation and the wide pH range in the gastrointestinal tract (GIT), as well as their limited absorption resulting from low GI epithelial permeability [1,3]. Additionally, oral drugs undergo hepatic first-pass metabolism, which further reduces their bioavailability [3]. An alternative route that can address the challenges associated with the aforementioned oral route is non-invasive IN delivery, which has been extensively studied for both localized and systemic drug delivery [4]. In recent years, this route has attracted attention due to its unique connection to the CNS via the olfactory and trigeminal pathways, enabling direct drug access to the brain bypassing the strict blood-brain barrier (BBB)– an advantage not offered by

* Corresponding author. Macquarie Medical School, Faculty of Medicine, Health and Human Sciences, Macquarie University, Sydney, NSW 2109, Australia.
** Corresponding author. Macquarie Medical School, Faculty of Medicine, Health and Human Sciences, Macquarie University, Sydney, NSW 2109, Australia.
E-mail addresses: huixin.ong@mq.edu.au (H.X. Ong), daniela.traini@mq.edu.au (D. Traini).

https://doi.org/10.1016/j.jddst.2025.107070
Received 7 January 2025; Received in revised form 4 May 2025; Accepted 21 May 2025
Available online 22 May 2025

conventional oral and parenteral routes [5]. Thus, the versatility of the IN route makes it a promising approach for treating a wide range of conditions, including nasal disorders, systemic diseases such as metabolic, endocrine and cardiovascular conditions, as well as neurological and inflammatory disorders [6,7]. Currently, several IN PPDs including insulin, insulin-like growth factor-1 (IGF-1), glucagon, calcitonin, oxytocin, vasopressin, glucagon-like peptide-1 and 2 (GLP-1 and GLP-2), human nerve growth factor (hNGF), human growth hormone (hGH), parathyroid hormone (PTH), leptin, ghrelin, erythropoietin (EPO), desmopressin, neuropeptide Y, brain-derived neurotrophic factor (BDNF), basic fibroblast growth factor (bFGF), and glial-derived neurotrophic factor (GDNF), are under investigation for potential systemic and CNS delivery [3,8–10].

Despite the benefits, the delivery of biomolecules through this route remains challenging, mainly due to their physicochemical properties (high molecular weight *i.e.*, >1000 Da, hydrophilic structure, surface charge, etc.) and the nasal physiological barriers such as low permeability of nasal epithelia, mucosa protease environment, rapid mucociliary clearance, short drug residence time, and limited administrable volume (25–200 μL), necessitating more frequent dosing [9,11–15]. As a result, regardless of the large mucosal surface area, rich vasculature of the nasal cavity, and the avoidance of hepatic first-pass metabolism [16], the bioavailability of peptides is generally between 1 % and 3 % [17,18].

Several strategies, including cell permeation enhancers, mucoadhesive systems, and nanocarriers, are being explored in nasal formulations to tackle the limitations linked to this route [7,14] and among these, nanoparticulate systems are considered one of the most promising approaches [4,19]. Nanoparticles (NPs) enhance drug solubility, elicit high drug absorption due to their greater surface area, protect encapsulated drugs from enzymatic degradation, increase the drug residence time at the absorption site, exhibit low mucociliary clearance, enhance bioavailability, and control the release rate of the drug. Additionally, NPs reduce dosing frequency, and minimize systemic side effects, for instance by reducing the drug distribution to unintended areas in case of localized and nose-to-brain (N2B) targeted drug delivery [12,14,20]. These highly organized nanostructures made from lipidic, polymeric, biological, or hybrid materials are used as potential drug carriers due to their unique and easily customizable properties [21]. Drugs can be attached to these carriers through conjugation or adsorption, or they can be entrapped within the carrier system [21]. Moreover, the carrier surface can be modified with appropriate ligands to improve target specificity [21]. Polymer-based drug carrier systems include polymeric NPs, colloidal carriers, polymer–drug conjugates, and smart polymer-based systems such as stimuli-sensitive hydrogels or *in situ* nasal gels [22,23]. In recent years, various biodegradable and biocompatible natural polymers (such as alginate, chitosan, silk) and synthetic polymers (including poly (lactic-*co*-glycolic acid) [PLGA], poly (acrylamide), poly (lactic acid) [PLA], poly (lysine), poly (acryl cyanoacrylate), poly (caprolactone), and poloxamer 407) have been explored as novel carrier systems for controlled and targeted drug delivery via the nasal route [2,22], thus showing the significant impact of nanobiotechnology in the field of drug delivery.

This study investigates a novel proprietary synthetic polymer, poly (N-isopropylacrylamide-*co*-(N-acryloxysuccinimide)-*co*-(polylactide/-hydroxy methacrylate)-*co*-(oligo (ethylene glycol), denoted as PNPHO, for IN PPD delivery. PNPHO is a thermoresponsive polymer with a molecular weight of ~70 kDa that undergoes *in situ* gelation at physiological temperature (37 °C) [24,25]. Additionally, this polymer is bioadhesive, biocompatible and has tunable biodegradability, exhibits structural stability, and elicits minimal inflammatory response, which makes it an ideal platform for drug delivery [24–26]. Its mucoadhesive property can prolong the residence time of the drug within the nasal mucosa [26], reducing drug elimination due to ciliary movement, enhancing drug bioavailability, lowering dosing frequency, and improving patient adherence to treatment [27]. This cost-effective polymer has proven to be clinically important as an injectable hydrogel for tissue regeneration and is being currently explored for a wide range of biomedical applications [24]. Furthermore, a recent study by Gholizadeh et al. investigated the role of the PNPHO polymer as a drug-delivery hydrogel platform for a broad range of compounds with different physicochemical properties [26].

BSA is one of the most widely used proteins in the evaluation of different drug delivery systems due to its cost-effectiveness, water solubility, stability, and availability [28,29]. Therefore, in the present study, BSA has been used as a model protein to explore PNPHO polymer's role as a nanocarrier for PPDs, as well as to assess how its thermoresponsive property can facilitate drug delivery following IN administration.

2. Materials and methods

2.1. Materials

PNPHO polymer was provided by Tetratherix Technology Pty Ltd, (Sydney, Australia). BSA, phosphate-buffered saline (PBS), Hanks' balanced salt solution (HBSS), CelLytic reagent, mucin type III from porcine stomach, and all HPLC-grade analytical solvents were purchased from Sigma Aldrich (Sydney, Australia). Water was deionized and purified by using a Milli-Q Reagent Grade water system (Merck Millipore, USA). Roswell Park Memorial Institute, RPMI 2650 cells (immortalised human nasal epithelial cell line derived from septum carcinoma) were purchased from the American Type Culture Collection (ATCC) (Virginia, USA). All cell culture reagents including Minimum essential medium (MEM), foetal bovine serum (FBS), trypsin, and non-essential amino acids were obtained from Gibco and Invitrogen (Sydney, Australia). SarGel® paste was purchased from Sartomer (Pennsylvania, USA), and MTS reagent was provided by Promega Corporation (Wisconsin, USA).

2.2. Methods

2.2.1. Microfluidic manufacturing of BSA-loaded PNPHO polymer NPs

BSA was dissolved in Milli-Q water to a concentration of 2 mg/mL. The PNPHO polymer was dissolved in PBS and kept at 4 °C overnight on a shaker to achieve concentrations of 40 mg/mL and 70 mg/mL. The BSA and the PNPHO solutions were injected into a 3D-printed T-shaped microfluidic device [30] through two separate inlets using 2 syringe pumps (Chemyx Fusion 200, Chemyx, Inc., USA) connected to the device via polytetrafluoroethylene (PTFE) tubing, facilitating passive micromixing inside a "zigzag" channel. The solutions were mixed in a 1:1 ratio at a total flow rate (TFR) of 10 mL/min, resulting in final concentrations of BSA 1 mg/mL + PNPHO 20 mg/mL and BSA 1 mg/mL + PNPHO 35 mg/mL in the NPs formulations. These polymer concentrations were selected for the study because it was observed that the polymer transitioned from liquid to gel at 37 °C starting at 20 mg/mL. The process of BSA-PNPHO NPs manufacture is illustrated in Fig. 1.

2.2.2. Characterization of BSA-PNPHO NPs

2.2.2.1. Particle size, PDI and zeta potential. The size, PDI and ζ-potential of the prepared NPs were measured at 25 °C using dynamic light scattering (DLS) Zetasizer Nano ZS (Malvern Panalytical, UK). The size of NPs is crucial in drug delivery, as it significantly impacts both drug cellular uptake and drug targeting efficiency [31]. The PDI determines the uniformity of particle sizes within a sample, with a value ranging from 0 to 1. A higher PDI suggests a broader size distribution with multiple particle size populations, which is undesirable [32]. A PDI value of <0.3 indicates a narrow particle size distribution and is considered suitable for IN formulations [33]. The ζ-potential reflects the surface charge of the NPs and also influences the cellular transport and stability of the biomolecules [33].

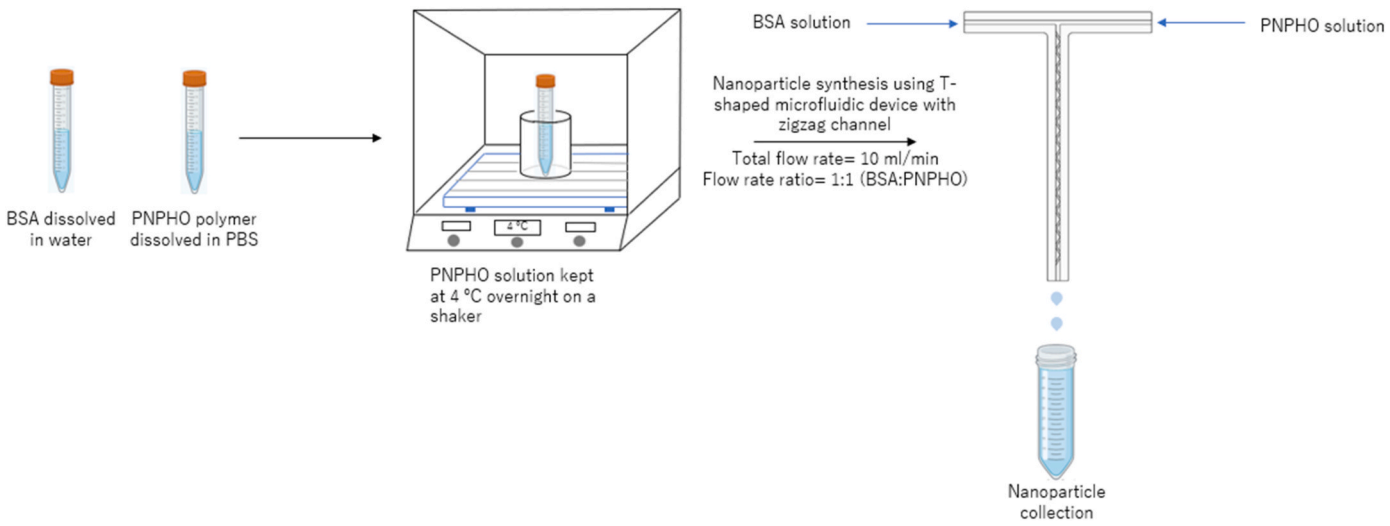

Fig. 1. Schematic representation of BSA-PNPHO nanoparticle formation using microfluidic method.

2.2.2.2. Encapsulation efficiency. The EE, *i.e.*, the amount of drug entrapped within the polymeric NPs, was determined as follows: 500 μL of the BSA-PNPHO formulations were added to the Amicon® Ultra-0.5 100 kDa molecular weight cut-off filter device (Merck Millipore, USA) placed into a microcentrifuge tube. The selection of the filter was based on the molecular weight of BSA, which is 66.5 kDa [29]. The samples were centrifuged at 14,000 rpm until there was no change in the volume of the filtrate. The volume of the filtrate was recorded. The filtrate containing the free BSA was further filtered through a 0.22-μm polyethersulfone syringe filter (Filter-Bio, China) prior to quantification of the drug by high performance liquid chromatography (HPLC). The percentage EE was calculated using the following equation [34]:

$$\%\ Encapsulation\ efficiency\ (\%\ EE) = \frac{Total\ mass\ of\ drug\ added - Mass\ of\ free\ drug}{Total\ mass\ of\ drug\ added} \times 100$$

2.2.2.3. Drug-polymer interaction study. To assess possible drug-polymer interaction, mass photometry measurements were acquired using a TwoMP mass photometer (Refeyn, UK). Mass photometry is a novel way to measure the mass of biomolecules. It works by quantifying the light scattered by an individual molecule in solution, which is directly proportional to its mass [35,36]. All mass photometry videos were recorded for 1 min and analysed using DiscoverMP (version 2022 R1).

Prior to sample analysis, mass calibration was performed according to the manufacturer's instructions using BSA. Briefly, 10 μL of 200 nM BSA was added to 10 μL of PBS in a sample well, and calibration was performed on peaks corresponding to BSA monomer, dimer and trimer (66, 132 and 198 kDa respectively). Calibration error was estimated at 4.5 %. For sample dilution and time series ('quick dilution') mass photometry analysis, 2 μL of each sample was added to 18 μL PBS in a sample well. Measurements commenced within ~3 s of sample addition and were collected for 6 min.

2.2.2.4. Physico-chemical stability and encapsulation efficiency retention study of the NPs. The NPs formulations (BSA 1 mg/mL + PNPHO 20 mg/mL and BSA 1 mg/mL + PNPHO 35 mg/mL) were assessed for changes in their physicochemical properties in terms of particle size, PDI, and ζ-potential. Additionally, the maintenance of EE was evaluated. A short-term stability study was performed by storing both formulations at 4 °C and at room temperature (20 °C) for a period of 28 days, with the abovementioned parameters measured on pre-determined days - Day 0, 1, 4, 7, 14, 21 and 28.

2.2.2.5. HPLC quantification method for BSA. BSA quantification was performed using an HPLC system (Shimadzu, Japan) equipped with an LC20AT pump, SIL20AHT autosampler, PD-20A UV–VIS detector, and LabSolution software. Chromatographic separation was performed using a reverse-phase (RP) C18 column of dimension: 250 mm × 4.6 mm and 5 μm particle size (Phenomenex, USA) with a gradient elution method and the column oven temperature set at 25 °C. The mobile phase was composed of 0.1 % trifluoroacetic acid (TFA) in Milli-Q water (Aqueous phase) and 0.1 % TFA in acetonitrile (Organic phase). Linearity was obtained for BSA standard solutions at concentrations ranging from 5 μg/mL to 200 μg/mL ($R^2 = 0.999$). Samples were diluted 10-fold to reach a concentration that falls within the standard concentration range. The analysis was performed at a detection wavelength of 220 nm using an injection volume of 20 μL and a flow rate of 1 mL/min with a retention time of 11 min.

2.2.2.6. Aerosol droplet size distribution. The size of aerosolized droplets from liquid formulations can vary depending on the type of nasal pumps and actuators used, as well as the characteristics of the formulations (*e.g.*, viscosity) [71]. In this study, a VP7 50 μL N2B targeting nasal spray device (Aptar Pharma) was used to generate the aerosols. The aerosolized BSA solution and NPs formulations released from the spray pump were evaluated for their droplet size distribution by laser diffraction using the Spraytec (Malvern Panalytical, UK). During this experiment, the tip of the nasal pump was positioned 6 cm from the measurement zone (laser beam) and was actuated manually at a 45-degree angle through the laser beam. The experiment was conducted in an open bench set-up with the measurement mode set to rapid. The particles were assessed with a dispersion refractive index of 1.0, particle refractive index of 1.33, and density of 1.0 g/cm^3, at a sampling frequency of 2.5 kHz using a 300 mm lens. The extractor was turned on during the

measurements to capture spray droplets and minimize bias to the results from aerosol re-entry into the measurement zone between actuations. Droplet size distribution corresponding to the 10th, 50th and 90th percentile of particles within the formulations represented as Dv10, Dv50, Dv90 respectively, percentage of respirable fraction (%< 10 μm), and Span value (particle size distribution width) were determined using Spraytec version 3.20 software.

2.2.2.7. Viscosity measurements. The viscosity of the aqueous BSA solution and the NPs formulations were measured at 25 °C using AR 2000 rheometer (TA Instruments, USA) to determine the effect of the rheological property of the respective samples on the droplet size. The measurements were performed using a cone-plate geometry with a diameter of 40 mm and a gap of 64 μm at shear rates ranging from 1 to 100 s^{-1}.

2.2.3. In vitro mucin/nanoparticle interaction

The mucoadhesive properties of the NPs formulations were investigated by monitoring changes in the surface charge of the NPs after incubation with mucin, as this glycoprotein is the primary component of the nasal mucus layer. Briefly, an aqueous stock solution of mucin type III (10 mg/mL) was prepared in PBS and stored at 4 °C. Mixtures were prepared at various NP:mucin ratios (1:0.025, 1:0.5, 1:1, 1:2, and 1:4 w/w) and incubated at 37 °C for 1 h in a thermo-shaker. Subsequently, the ζ-potential of all the samples were measured. Control samples included mucin at all tested concentrations and NPs formulations without mucin.

2.2.4. In vitro nasal drug deposition study

2.2.4.1. Silicone human nasal cast deposition semi-quantitative measurements. The drug deposition behaviour of the BSA solution and NPs formulations into the nasal cavity was studied using a transparent silicone human nose model (Koken Co. Ltd., Japan), to mimic human nasal deposition. The inner surface of the nasal cast was coated with 0.5 gm SarGel® moisture-sensitive paste evenly to visualize the deposition area, represented by a purple colour change on exposure to aerosol droplets. The coated nose model was allowed to equilibrate for 20 min at 37 °C in a dry-sealed box with silica gel prior to starting the experiment. The VP7 nasal spray device was used to deliver BSA 1 mg/mL and the formulations. The device was inserted into the nostrils of the cast at a depth of 5 mm (maximum depth available) and manually actuated once at two different angles - 45° and 70° from the horizontal plane to release a volume of 50 μL per spray from the delivery device, followed by incubation for 20 min in a sealed dry box with silica gel. Spray angles of 45° and 70° were used to assess potential differences in drug deposition based on the device orientation. The nose model was positioned vertically both during actuation and incubation. Images were captured every 5 min and the areas of different regions of the nasal cast covered by the sprayed samples were analysed using Fiji ImageJ software (https://imagej.net). During the analysis, the segmentation of each region of the nasal cast was performed as described by D'Angelo et al. [37].

2.2.4.2. Alberta nasal cast drug deposition measurements. The nasal deposition of the free BSA drug and BSA-PNPHO NPs formulations was further evaluated using the Alberta Idealized Nasal Inlet (AINI) coupled with next-generation impactor (NGI) (Copley Scientific, UK). The AINI model enables quantitative estimation of drug deposited in different parts of the nasal cavity [38]. In this experiment, an inspiration flow rate of 15 L/min was used, which is a representative flow rate for most of the nasal deposition studies, and the particle cut-off diameter of the NGI stages at this flow rate was 14 μm and below as it progresses from Stage 1 to Stage 8 [38]. The nasal spray device was positioned at 45° and 70° relative to the horizontal surface at an insertion depth of 5 mm into the nostril during actuation. Each sample was subjected to 10 sprays to recover a quantifiable amount of drug from each nasal region, including the olfactory region which is difficult to access. The AINI regions comprising nostril, turbinates, olfactory region, and nasopharynx and the NGI stages with 8 collection cups were dis-assembled after spraying followed by rinsing of the individual parts with Milli-Q water to recover the BSA deposited in each part of the nasal cast and NGI collection cups, which was quantified using validated HPLC method.

2.2.5. Cytotoxicity study on RPMI 2650 nasal epithelial cells

For the cytotoxicity study, human nasal epithelial cells RPMI 2650 were cultured in MEM supplemented with 10 % (v/v) FBS and 1 % (v/v) non-essential amino acid solution and incubated at 37 °C in 5 % CO_2 and 95 % relative humidity (RH). After reaching approximately 90 % confluency, the cells were seeded at a density of 5×10^5 cells/mL per well in 96-well plates (Corning Costar, USA) and allowed to adhere. BSA solution, PNPHO polymer solutions, and both the BSA-PNPHO formulations were diluted in cell medium to obtain BSA 1 mg/mL, PNPHO 20 mg/mL, PNPHO 35 mg/mL and formulations of corresponding concentrations in the final volume. After 24 h, the cells were treated with 100 μL of the samples at the concentrations specified and incubated for another 24 h. The treatment samples were removed from the wells and cells were exposed to the MTS reagent (1:5 v/v MTS: cell medium) for 3 h. The absorbance was measured at a wavelength of 490 nm using the SpectraMax ID3 microplate reader (Molecular Devices, USA).

2.2.6. Transepithelial drug transport, transepithelial electrical resistance measurement and Flu-Na permeability study

2.2.6.1. Drug transport study. The RPMI 2650 cells with a seeding density of 2.5×10^6 cells/mL were cultured on the apical side of Snapwell cell culture inserts (Corning Costar, USA) coated with a polyester membrane (0.4 μm pore size, 12 mm diameter insert) in 6-well plates at 37 °C and 5 % CO_2. The cells were initially grown in 200 μL cell media on the apical side of the insert and the insert was submerged in 2 mL cell media on the basolateral side. After 48 h, the apical medium was aspirated and the basal medium was replenished with fresh cell medium every second day to facilitate the growth of nasal cells at the air-liquid interface (ALI) for 14 days. For the drug transport study, Snapwell inserts containing cells were fitted into a 3D printed modified expansion chamber connected to NGI as described by Pozzoli et al. [39] and BSA solution and NPs formulations aerosolized at a flow rate of 15 L/min, as illustrated in Fig. 2. The inserts were then placed back into the wells with 2 mL HBSS in the basolateral chamber and incubated for 4 h to conduct the transport study. During this 4-h transport study, 200 μL of samples were withdrawn from the basolateral compartment at regular time intervals (0.5, 1, 1.5, 2, 2.5, 3 and 4 h) and replaced with an equal volume of pre-warmed HBSS to maintain sink conditions. At the end of the experiment, the cells were washed gently with HBSS to collect and quantify the amount of drug remaining on the cell surface. CelLytic reagent was used to lyse the cells and determine the amount of drug present inside the cells. All the samples were analysed using HPLC method described in Section 2.2.2.5.

2.2.6.2. Assessment of cellular integrity using TEER measurements and Flu-Na permeability of RPMI 2650 cells. Transepithelial electrical resistance (TEER) measurement is used to assess the barrier integrity of the epithelial cell monolayers that is highly regulated by the tight junction proteins [7,39,40]. The TEER of the RPMI 2650 nasal cells was measured using EVOM2 Voltohmmeter (World Precision Instruments, Sarasota, USA) before and after 4 h of treatment with the BSA solution and NPs formulations (Fig. 2) as previously described by Baldelli et al. [41]. The TEER (Ω.cm^2) values for the control (cells without treatment) and treatment groups were calculated using the following equation [40]:

$$TEER = (R_{TEER} - R_{Blank}) \times A_{Membrane}$$

where R_{TEER} is the resistance of the membrane with cells for control and

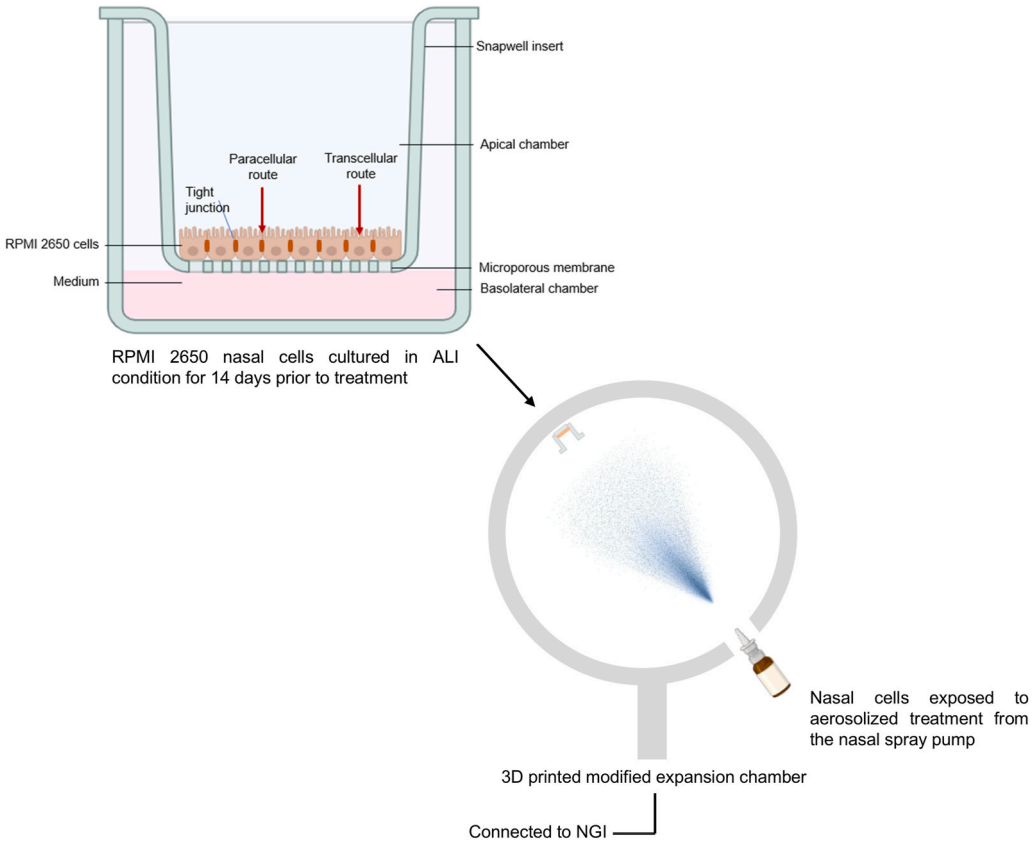

Fig. 2. Schematic illustration of the experimental setup for RPMI 2650 nasal cell treatment in a 3D printed modified expansion chamber.

treatment groups, R_{Blank} is the resistance of the membrane without a cell monolayer and $A_{Membrane}$ is the membrane surface area of the Snapwell insert (1.12 cm^2).

Following the TEER measurement, 200 μL of pre-warmed fluorescein sodium (Flu-Na) solution (2.5 mg/mL), a well-known marker for the assessment of paracellular transport [39], was added to the apical side of the Snapwell plate and incubated at 37 °C and 5 % CO_2 for 60 min. 200 μL of samples were collected from the basolateral chamber at regular time intervals (15, 30, 45 and 60 min). After the withdrawal of each sample, an equal volume of fresh pre-warmed HBSS was added. Flu-Na standard solutions were prepared at concentrations ranging from 0.00125 μg/mL to 250 μg/mL. The standard solutions and the samples were added to clear flat bottom black 96 well plates (Corning, USA). The fluorescence intensity of Flu-Na was detected using SpectraMax ID3 microplate reader (Molecular Devices, USA) at excitation λ of 485 nm and emission λ of 538 nm. The apparent permeability coefficient (Papp, cm/s) of Flu-Na was calculated using the following equation [40]:

$$P_{app} = \frac{dQ}{dt} \times \frac{1}{C_0 A}$$

where dQ/dt is the flux of Flu-Na (μg/s) across the membrane, C_0 is the initial Flu-Na concentration (μg/ml) in the donor compartment, and A (cm^2) is the membrane surface area of the Snapwell insert (1.12 cm^2).

2.2.7. Drug release kinetics study

The drug release kinetics from the polymeric system were evaluated using *in vitro* drug transport data from the RPMI 2650 nasal cell line, which closely simulates the nasal environment. To analyse the release kinetics and elucidate the underlying release mechanism, the data were fitted into various mathematical models, including zero order, first order, Higuchi, and Korsmeyer-Peppas models.

The zero-order model (Eq. (1)) describes the systems where the rate of drug release is independent of its concentration [42].

$$C = k_0\, t \qquad \text{(Eq. 1)}$$

where C = concentration of drug at time 't'
t = time
k_0 = zero order rate constant expressed in units of concentration/time

The first-order model (Eq. (2)) explains the release from systems where the drug release rate is concentration dependent [42].

$$Log\, C = Log\, C_0 - k_1 t / 2.303 \qquad \text{(Eq. 2)}$$

where C_0 = initial concentration of drug
k_1 = first order rate constant

The Higuchi model (Eq. (3)) explains the release of drugs from an insoluble matrix as a square root of time-dependent process based on Fickian diffusion [42].

$$C = K_H\, t^{1/2} \qquad \text{(Eq. 3)}$$

where K_H = constant reflecting the design variables of the system

The Korsmeyer-Peppas model (Eq. (4)) is generally used to describe the drug release from a polymeric system [42].

$$Log\,(M_t / M_\infty) = Log\, K_{KP} + n\, Log\, t \qquad \text{(Eq. 4)}$$

where M_t/M_∞ = fraction of drug released at time 't'
K_{KP} = rate constant
n = release exponent

2.2.8. Statistical analyses

All the experiments were conducted in triplicate and results expressed as mean ± standard error of the mean (SEM). Statistical data analyses were performed by two-way analysis of variance (ANOVA)

with Tukey's post-test using GraphPad Prism (version 10.2.2) with a *p*-value less than 0.05 considered as statistically significant.

3. Results and discussion

3.1. Characterization of BSA-PNPHO NPs

3.1.1. Size, PDI, ζ-potential, and encapsulation efficiency of the NPs formulations

The BSA NPs were characterized in terms of particle size, PDI, ζ-potential, and drug EE.

Particle size is crucial for achieving targeted drug delivery and hence, minimizes systemic side effects [31]. Although nasal drug delivery offers rapid absorption and high bioavailability, most PPDs are not well absorbed across the nasal mucosa due to their low permeability [43]. Nanoparticulate systems have been particularly useful for biopharmaceuticals that have low epithelial cellular permeability [44]. Currently, no evidence regarding the optimal particle size is available for effective nasal drug delivery for systemic use and N2B delivery. However, studies suggest that to successfully cross the N2B epithelial barrier, the particle size should generally be less than 200 nm [31,33,45–48]. Moreover, the transport of therapeutic agents across the olfactory epithelium to the olfactory bulb (OB) and subsequently to the brain occurs through different processes, depending on their size [49]. If the size is between 10 nm and 300 nm, the NPs can deliver the therapeutic agents directly to the brain via the olfactory region [49]. Particles <200 nm are taken up via clathrin-dependent endocytosis, while those between 100 nm and 200 nm are transported by caveolae-mediated endocytosis [49]. Most of the peptide- or protein-loaded NPs studied for N2B delivery typically fall within the size range of 50–150 nm, however, particles as large as 440 nm have also been successfully delivered to the brain [14]. In the current study, the average particle sizes of the BSA 1 mg/mL + PNPHO 20 mg/mL and BSA 1 mg/mL + PNPHO 35 mg/mL NPs formulations were found to be 28.32 ± 0.09 nm and 39.64 ± 0.31 nm, respectively, which fall within the suitable range of drug delivery to the systemic circulation and brain. The increase in particle size with higher polymer concentration was statistically significant ($p < 0.05$).

For IN formulations, a PDI value of <0.3 is typically recommended [33]. In this study, both NPs formulations exhibited PDI values ranging from 0.25 to 0.39, indicating a narrow particle size distribution and suggesting that the particles are monodispersed and suitable for nasal aerosolization.

ζ-potential is an important index for drug uptake and physical stability of NPs formulations [33]. The BSA-PNPHO NPs demonstrated ζ-potential values between −3 mV and −5 mV, reflecting an overall negative surface charge. While NPs with a positive ζ-potential tend to enhance and prolong drug retention in the nasal mucosa owing to the electrostatic interaction with negatively charged mucin residues, however, they can also induce cytotoxicity, potentially leading to nasal irritation and subsequently injury [14]. Some studies have shown that the use of certain anionic nanocarriers resulted in improved permeability across the olfactory epithelium based on their surface chemical composition compared to positively charged carriers such as chitosan [14,33]. These results can be correlated with our study that shows that the NPs produced with a negative surface charge may consist of a chemical moiety responsible for the mucoadhesivity of the polymer, and thus could facilitate controlled and effective drug delivery to the target tissues [50].

The EE for both NPs formulations was found to be approximately 86 %, indicating that a significant fraction of the active drug is effectively incorporated into the nanocarriers, which is critical for maximizing

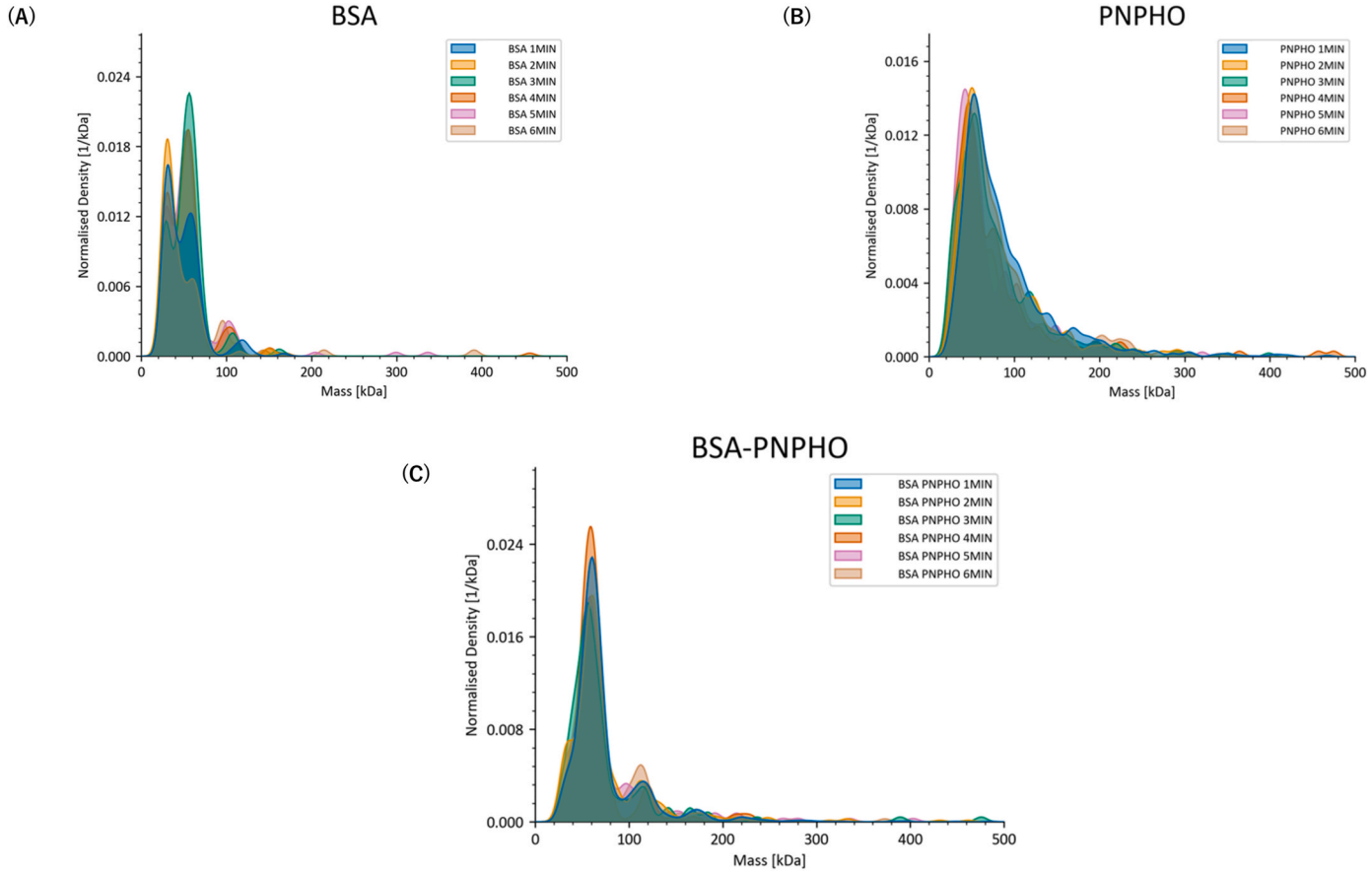

Fig. 3. BSA-PNPHO interaction study using mass photometry. Time course analyses for (A) BSA (B) PNPHO and (C) BSA-PNPHO.

therapeutic efficacy. This is particularly important for N2B drug delivery, where achieving an adequate concentration to the olfactory region, which constitutes only a small portion of the nasal cavity [51], is essential for efficacy. Moreover, encapsulating the PPDs in polymeric NPs provides drug protection against protease environment, enhancing their stability [52]. Additionally, a high EE ensures less drug wastage and effective utilization of the active ingredient, potentially lowering production costs [53].

3.1.2. Drug-polymer interaction study

The individual time course analyses of the possible drug-polymer interaction for each sample are presented in Fig. 3. From the results it can be observed that the ~40 kDa peak in the BSA sample (Fig. 3A) is consistently missing from each time point of the BSA-PNPHO sample analysed (Fig. 3C), suggesting interaction between the drug and the polymer under the experimental conditions. However, further complementary techniques (*e.g.*, isothermal titration calorimetry, nuclear magnetic resonance) are needed to confirm the nature and strength of the interaction. The interaction indicated by the observed mass shift in the mass photometry data potentially may enable controlled drug release by modulating the drug's dissolution or diffusion rates. Furthermore, drug-polymer complexes could improve bioavailability by protecting the drug from degradation.

3.1.3. Physico-chemical stability and encapsulation efficiency retention study of the NPs

The changes in the physicochemical properties of NPs formulations were evaluated by comparison of the size, PDI, and ζ-potential over a period of 28 days after storage at 4 °C and 20 °C (Fig. 4). No significant changes were observed in these parameters during the experimental period when stored at 4 °C, with average sizes maintained at around 28 nm and 39 nm, respectively, PDI< 0.4, and ζ-potential between −3 mV and −6 mV. A greater fluctuation in size and ζ-potential of the NPs was observed when stored at 20 °C. At this higher temperature, the size of the NPs was observed to increase significantly from Day 14 onwards. This change may be attributed to particle agglomeration upon long-term storage at higher temperatures, while the lower temperature prevents particle collision and agglomeration due to reduced kinetic energy [54]. Additionally, at lower temperature, the polymer adopts a coiled chain structure, which is less prone to degradation. As the temperature increases, the polymer is in the process of degradation, gradually transitioning to a globular structure, leading to the formation of agglomerates over time. Furthermore, both NPs at room temperature drifted towards the positive charge over time.

Table 1
Encapsulation efficiency of NPs formulations at 4 °C and 20 °C for a period of 4 weeks.

Encapsulation efficiency (%)				
Day (s)	BSA 1 mg/mL + PNPHO 20 mg/mL		BSA 1 mg/mL + PNPHO 35 mg/mL	
	4 °C	20 °C	4 °C	20 °C
D0	85.59 (±0.15)	–	86.55 (±0.46)	–
D1	89.06 (±0.06)	92.26 (±0.16)	91.38 (±0.03)	8.19 (±1.03)
D4	91.57 (±0.07)	95.23 (±0.04)	92.24 (±0.29)	36.79 (±0.32)
D7	89.70 (±0.08)	92.36 (±0.16)	92.13 (±0.02)	28.05 (±3.59)
D14	94.53 (±0.18)	29.43 (±4.66)	96.14 (±0.018)	30.72 (±0.43)
D21	87.75 (±0.20)	white agglomerates	91.68 (±0.004)	white agglomerates
D28	90.73 (±0.04)		94.21 (±0.12)	

Data is expressed as mean (±SEM), n = 3.

The polymer's ability to maintain BSA entrapment was assessed over a period of 4 weeks (Table 1). The EE was retained within a range of 86 %–96 % for both NPs formulations at 4 °C throughout the study period. However, for BSA 1 mg/mL + PNPHO 20 mg/mL, the EE significantly dropped from 92 % to 29 % by Day 14 at 20 °C. Similarly, the EE of BSA 1 mg/mL + PNPHO 35 mg/mL decreased to 30 % by Day 14 at 20 °C. Both the formulations formed white agglomerates at 20 °C post Day 14. This infers that the NPs formulations should be stored at 4 °C to maintain their physical stability.

3.1.4. Aerosol droplet size distribution

Determining the droplet size distribution is important not only for evaluating the nasal deposition efficiency of the aerosol produced by the nasal spray device but also for complying with the FDA guidelines that restrict the unwanted deposition of a fraction of small droplets in the

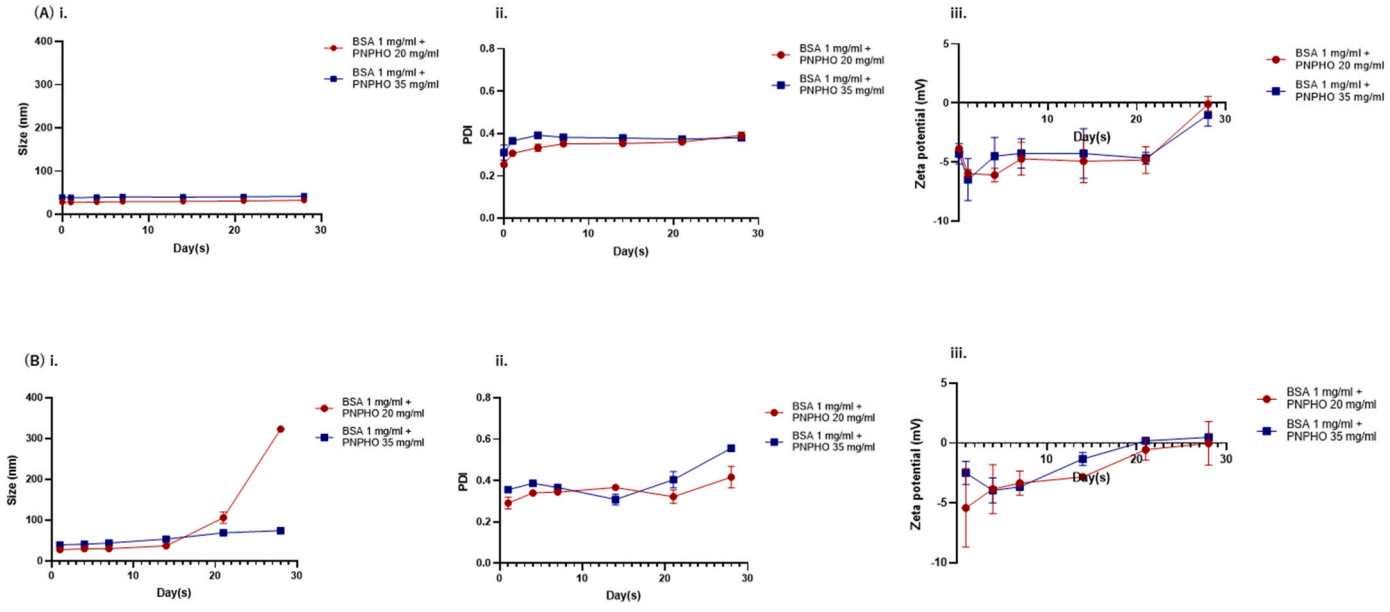

Fig. 4. Short-term stability study of BSA-PNPHO NPs formulations stored at (A) 4 °C and (B) room temperature (20 °C). Samples were evaluated in terms of size (i), PDI (ii), and zeta potential (iii) for a period of 28 days. The results are represented as mean ± SEM (n = 3).

Table 2
Aerosol droplet size distribution.

	BSA 1 mg/mL	BSA 1 mg/mL + PNPHO 20 mg/mL	BSA 1 mg/mL + PNPHO 35 mg/mL
Dv (10) (μm)	47.70 (±1.22)	73.64 (±1.90)	70.43 (±2.64)
Dv (50) (μm)	147.77 (±1.28)	218.07 (±3.08)	237.23 (±13.13)
Dv (90) (μm)	373.00 (±13.35)	567.03 (±27.52)	643.67 (±19.60)
%V < 10 μ (%)	0.09 (±0.05)	0.004 (±0.004)	0.05 (±0.01)
Span	2.20 (±0.08)	2.26 (±0.11)	2.42 (±0.07)

Data is expressed as mean (±SEM), n = 3.

lungs from the nose [55,56]. In general, Dv50 for nasal spray is between 30 μm and 120 μm [57]. If the droplet size is too fine (<10 μm) there is a possibility that the particles will pass through the nasal passages and deposit in the lungs, which can result in undesirable effects [57,58]. On the other hand, if the droplet size is too large (>120 μm), the spray may be trapped in the nostrils [57,58].

Table 2 shows the Dv10, Dv50, Dv90, and Span values generated upon actuation of the BSA solution and NPs formulations at 45° angle. Both Dv50 and Dv90 were significantly higher for the NPs formulations compared to the BSA solution alone ($p < 0.01$), due to the presence of the PNPHO polymer in the formulations. It was also observed that the droplet size becomes larger with increase in polymer concentration from 20 mg/mL to 35 mg/mL. The median droplet size *i.e.*, Dv50 of the aerosols for the BSA solution and formulations was found >120 μm, indicating the aerosols are most likely to deposit on the anterior parts of the nose upon actuation, and can be quickly removed by sneezing or mucociliary clearance [56,59]. A negligible respirable fraction (droplets <10 μm) was observed for all samples, minimizing aerosol deposition to the lungs.

3.1.5. Viscosity measurements

As the rheological behaviour of nasal formulations influences their spray characteristics [58], the viscosity of the NPs formulations were measured at 25 °C and compared to the aqueous BSA solution as the control. Both BSA and NPs formulations exhibited a very low viscosity of 0.00224 Pa.s (for control formulation containing BSA only), 0.00163 Pa.s (for BSA with PNPHO 20 mg/mL formulation), and 0.00205 Pa.s (for BSA with PNPHO 35 mg/mL formulation), respectively. Some studies reported that nasal formulations with higher viscosity is associated with larger droplet size [58]. However, in the current study, the viscosity levels were not high enough to produce such large droplets for all samples (Table 2). Notably, a directly proportional correlation was observed between polymer concentration and viscosity. Interestingly, the Dv50 of the free drug was lower, while its viscosity was higher

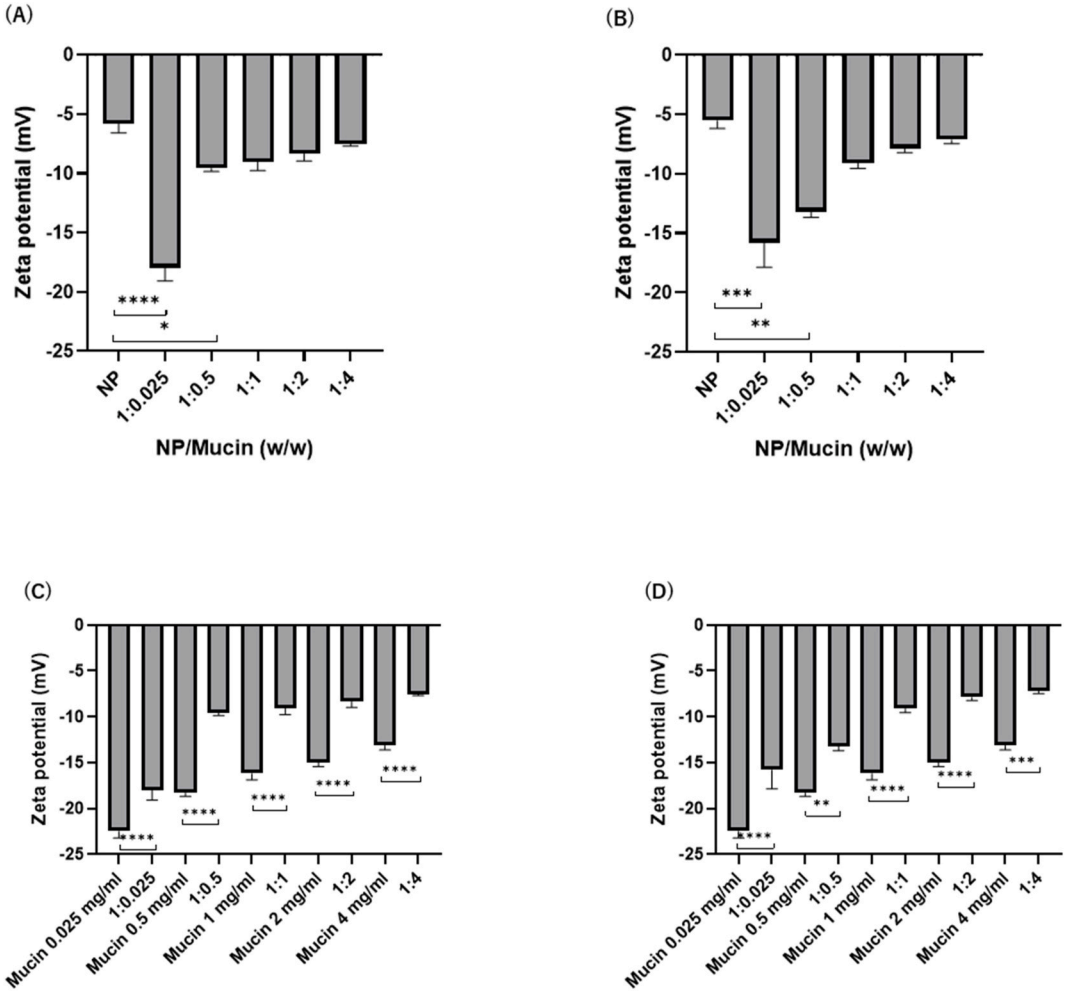

Fig. 5. Mucin-nanoparticle interaction. (A) ζ-potential measurements of BSA 1 mg/mL + PNPHO 20 mg/mL without mucin (NP) and with mucin at varying NP: mucin ratios (B) ζ-potential measurements of BSA 1 mg/mL + PNPHO 35 mg/mL without mucin (NP) and with mucin at varying NP:mucin ratios (C) Comparison of surface charge between BSA 1 mg/mL + PNPHO 20 mg/mL with mucin and mucin alone (D) Comparison of surface charge between BSA 1 mg/mL + PNPHO 35 mg/mL with mucin and mucin alone. (n = 3, mean ± SEM), *, p-value <0.05, **, p-value <0.01, ***, p-value <0.001, ****, p-value <0.0001.

compared to the formulations, which did not exhibit a similar correlation.

3.2. In vitro mucin/nanoparticle interaction

The ζ-potential of the mucin-NP complexes was measured to evaluate the mucoadhesive characteristics of the PNPHO polymer encapsulating BSA. As shown in Fig. 5A and B, the surface charge of the NPs became more negative upon incubation with mucin at NP:mucin ratios of 1:0.025 and 1:0.5 for both formulations, compared to the NPs without mucin. The observed shifts in ζ-potential were statistically significant, indicating an interaction between the mucin and the NPs. However, as the mucin concentration increased further, a decrease in the negative ζ-potential was noted, suggesting that the mucin may begin to saturate the available surface binding sites on the NPs, thereby shielding the NP surface charge at higher ratios and reducing the overall electrostatic interactions between the mucin and the NPs. Additionally, when the ζ-potential of the mucin-NP complexes was compared with that of mucin at corresponding concentrations (Fig. 5C and D), a statistically significant difference was observed. This further infers that the changes in the surface charge of the NPs are due to the adsorption of mucin onto the NP surface. Furthermore, NPs with a more negative ζ-potential than the mucin may experience electrostatic repulsion, leading to weaker or no mucoadhesion. In contrast, NPs with a charge similar to or slightly less negative than mucin may interact more favourably with mucin, promoting mucoadhesion. These interactions are crucial for overcoming mucociliary clearance, thereby prolonging the drug residence time on mucosal surface and enhancing its bioavailability following IN administration.

Compared to cationic NPs, which typically exhibit stronger mucoadhesion and enhanced paracellular transport by transiently opening epithelial tight junctions (*e.g.*, chitosan) [60], anionic systems generally display weaker binding to mucin [61], resulting in reduced nasal residence time. However, despite the lower surface charge of the NPs used in this study, the sol-gel transition of the thermoresponsive PNPHO polymer at physiological temperature may partially compensate for the limited nasal mucosal interaction by reducing mucociliary clearance, thereby prolonging drug residence time. Moreover, although cationic systems provide improved adhesion, they are often associated with epithelial toxicity or irritation, especially upon repeated administration, raising safety concerns [62]. Therefore, in this context, the PNPHO polymer's biocompatibility renders it a safer option compared to these cationic polymers.

3.3. In vitro nasal drug deposition study

3.3.1. Silicone human nasal cast

A transparent silicone nasal cast was used to evaluate the regional deposition of the formulations in the nasal cavity 20 min after actuation of the Aptar VP7 N2B targeting nasal spray device at 45° and 70° angles to the horizontal, and results compared with free BSA solution. The area covered was analysed by segmenting each region of the nasal cavity, as illustrated in Fig. 6, with the coverage for each region calculated as a percentage of the total surface area of that region (Table 3). Compared to the free drug (14.74 ± 0.58 % vs 13.26 ± 3.11 %), the NPs formulations demonstrated greater coverage of the total nasal cavity (16.60 ± 0.45 % vs 16.96 ± 0.98 % and 24.16 ± 1.98 % vs 22.60 ± 0.31 %) at both spray angles, with coverage increasing as polymer concentration rose. For the BSA only, drug deposition was predominantly observed in the nostrils, followed by the olfactory region and turbinates at the 45° spray angle. In contrast, both NPs formulations showed a similar deposition pattern across all three regions, at their respective concentrations. At the 70° spray angle, the nostrils and olfactory region had higher coverage than the turbinates for all three samples.

The area of the olfactory region covered by BSA 1 mg/mL + PNPHO 35 mg/mL (40.88 ± 0.62 %) was found to be greater than that of BSA 1 mg/mL (30.42 ± 0.14 %) and BSA 1 mg/mL + PNPHO 20 mg/mL (20.10 ± 3.87 %) at 45°, with the increase being statistically significant (Table 3 and Fig. 7). This suggests that the NPs formulation containing 35 mg/mL of polymer achieves more targeted deposition in the olfactory region, likely due to its thermosensitive nature at 37 °C, enabling mucoadhesivity to the target area at this higher concentration and enhances its surface retention relative to the free drug and NPs formulation with a lower polymer concentration at 20 min time point. These results indicate the potential of the polymer at higher concentrations to facilitate N2B drug delivery. In contrast, there is no notable difference in olfactory area coverage among the three samples at 70° spray angle (Table 3 and Fig. 7), with a similar deposition pattern.

Regardless of the variation in nasal spray administration angles, no significant difference in the total area coverage of the nasal cavity and other nasal sections was observed, except for BSA 1 mg/mL + PNPHO 20 mg/mL, which demonstrated a significant increase in olfactory area coverage at 70° compared to 45°, as depicted in Fig. 7. Deposition of BSA and the NPs formulations appeared to be negligible in the nasopharynx at both angles, suggesting the samples are less likely to deposit in the lower airways.

3.3.2. Alberta nasal cast deposition

The drug recovered from each section of the Alberta nasal cast was evaluated at 45° and 70° angles, as illustrated in Fig. 8. At 45° spray angle, only a small fraction of the drug administered *i.e.*, ~0.5 %–0.8 % reached the olfactory area and the difference in deposition between BSA and the NPs formulations was not statistically significant. The low drug deposition in the olfactory area may be since it comprises only a small portion of the nasal cavity and requires the drug to navigate through a narrow nasal airway passage, which is difficult to access [7].

For the BSA only, the drug predominantly deposited in the turbinates (67.33 ± 1.13 %), followed by the nasopharynx (25.15 ± 0.45 %), nostril (6.78 ± 0.51 %), and olfactory region (0.75 ± 0.18 %). In contrast, both the NPs formulations primarily deposited in the nasopharynx (63.12 ± 1.50 % and 61.22 ± 2.76 %), followed by the turbinates (27.64 ± 0.72 % and 30.82 ± 3.24 %), nostril (8.38 ± 0.79 % and 7.36 ± 0.44 %), and olfactory region (0.85 ± 0.01 % and 0.59 ± 0.04 %).

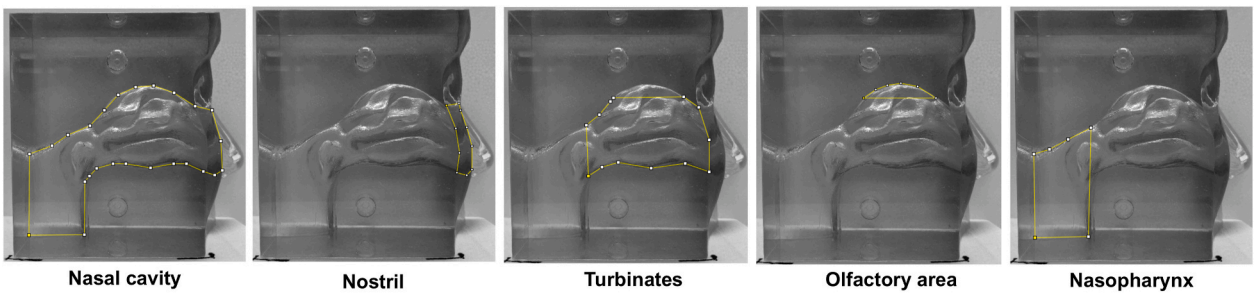

Fig. 6. Segmentation of different regions of the silicone human nose model for *in vitro* drug deposition analysis.

Table 3
Area coverage data for different regions of the silicone nasal cast.

	Region area coverage (%)					
	Spray angles	Total nasal cavity	Nostril	Turbinates	Olfactory region	Nasopharynx
BSA 1 mg/mL	**45°**	14.74 (±0.58)	41.67 (±4.22)	21.18 (±0.92)	30.42 (±0.14)	0 (±0)
	70°	13.26 (±3.11)	35.39 (±13.68)	18.48 (±4.42)	34.09 (±1.66)	0 (±0)
BSA 1 mg/mL + PNPHO 20 mg/mL	**45°**	16.60 (±0.45)	25.39 (±2.06)	25.30 (±0.47)	20.10 (±3.87)	0 (±0)
	70°	16.96 (±0.98)	33.33 (±2.15)	24.45 (±3.00)	34.30 (±0.53)	0 (±0)
BSA 1 mg/mL + PNPHO 35 mg/mL	**45°**	24.16 (±1.98)	36.67 (±3.82)	36.43 (±4.62)	40.88 (±0.62)	0.43 (±0.43)
	70°	22.60 (±0.31)	45.15 (±0.86)	34.20 (±1.05)	36.62 (±0.80)	0.64 (±0.64)

The coverage for each region was calculated as a percentage of the total surface area of that specific region. Data is expressed as mean (±SEM), n = 3.

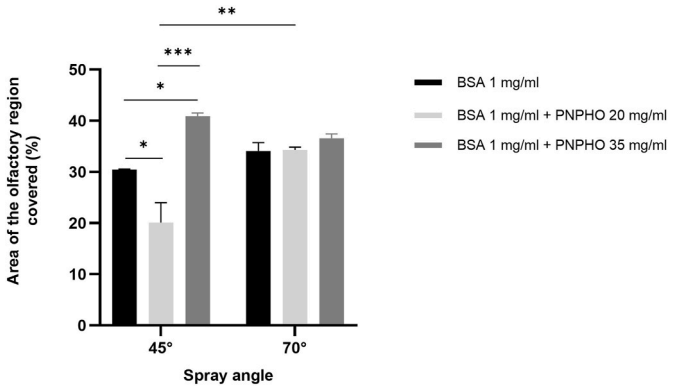

Fig. 7. Graphical representation of the percentage area of the olfactory region covered at 20 min post actuation of BSA 1 mg/mL and the NPs formulations from the VP7 nasal delivery device at 45° and 70° angles to the horizontal plane. (n = 3, mean ± SEM), *, p-value <0.05, **, p-value <0.01, ***, p-value <0.001.

At a spray angle of 70°, the formulation with PNPHO 20 mg/mL showed only 0.36 ± 0.36 % deposition in the olfactory region, and no drug deposition was observed in the target area for either the BSA solution or the PNPHO 35 mg/mL containing formulation, which may be attributed to the drug concentration falling below the detection limit. At this spray angle, the free BSA aerosol droplets predominantly deposited in the turbinates (66.91 ± 3.15 %), followed by the nasopharynx (19.76 ± 2.48 %), and nostril (13.33 ± 5.63 %). The NPs formulations mostly deposited in the turbinates (53.85 ± 12.14 % and 64.94 ± 9.25 %), with similar amounts reaching both the nasopharynx (20.75 ± 2.67 % and 19.02 ± 0.84 %) and nostril (25.04 ± 15.18 % and 16.03 ± 10.08 %). No drug was detected in the NGI stages for either of the samples, suggesting these NPs formulations can be suitable for nasal delivery.

While the silicone and Alberta nasal casts used in this study offer valuable insights into regional deposition patterns of the NPs formulations, they do not fully replicate the physiological complexity of the human nasal cavity. Specifically, they lack dynamic factors such as mucociliary clearance, enzymatic degradation, local immune responses, variations in nasal airflow due to breathing patterns or posture, and interindividual anatomical variability [63,64]. As a result, these static *in vitro* models may overestimate nasal deposition or retention compared to *in vivo* conditions, limiting their predictive accuracy for human nasal drug delivery and N2B targeting. Nevertheless, the casts encompass key anatomical regions, including the vestibule, turbinates, olfactory region, and nasopharynx, making them more physiologically representative than simpler models. They remain a valuable and cost-effective preclinical tool for evaluating IN deposition and enabling rapid optimization of IN drug formulations.

3.4. Cytotoxicity study of RPMI 2650 nasal epithelial cells

The cytotoxicity of BSA, PNPHO at varying concentrations, and NPs formulations were evaluated in RPMI 2650 cells using the MTS assay. The cell viability threshold was set to <70 % compared to the negative control group (cells without treatment) according to ISO 10993–5, for the samples to be considered cytotoxic.

The cell viability for all treatment samples was found to be above 70 % as shown in Fig. 9, indicating that none of the treatments elicited toxicity at the concentrations used.

3.5. Transepithelial drug transport, TEER measurement and Flu-Na permeability study

The RPMI 2650 cells grown under ALI conditions were treated with BSA alone and with formulations containing PNPHO to evaluate the polymer's effect on drug permeation across the cells compared to unencapsulated BSA. Approximately 60 % of the BSA drug was

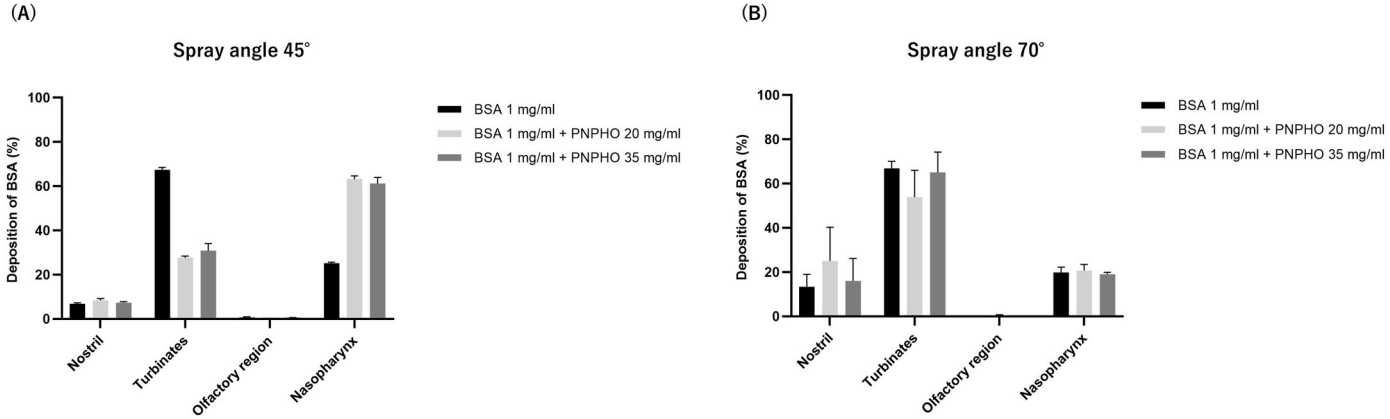

Fig. 8. Graphical representation of *in vitro* drug deposition in various regions of Alberta nasal cast. BSA 1 mg/mL and the NPs formulations were delivered to the nasal cavity using VP7 nasal spray pump positioned at (A) 45° and (B) 70° angles to the horizontal plane. Each sample was subjected to 10 actuations per run. (n = 3, mean ± SEM).

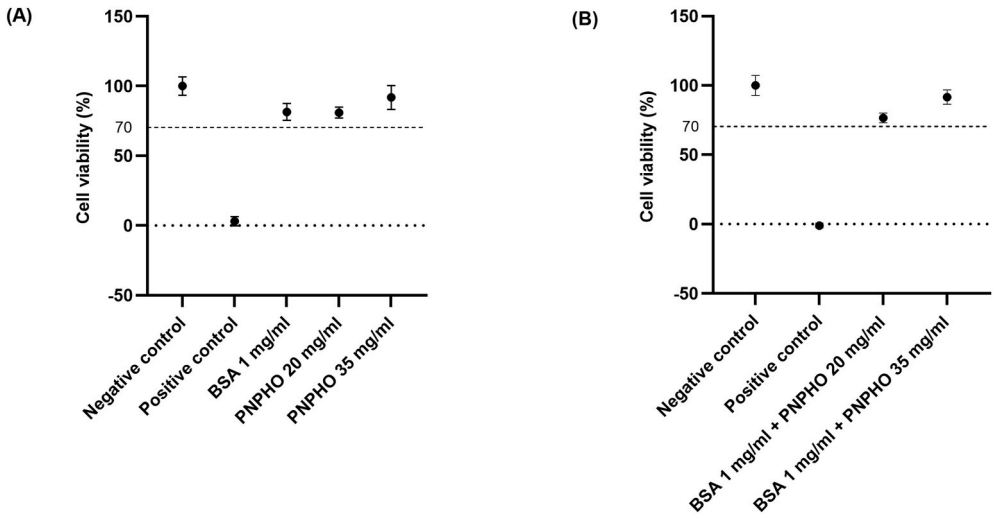

Fig. 9. The percentage of cell viability of RPMI 2650 cells upon exposure to (A) BSA 1 mg/mL and PNPHO at different concentrations and (B) BSA + PNPHO NPs formulations, for 24 h assessed by the MTS assay. The negative control represents untreated RPMI 2650 cells. The positive control represents RPMI 2650 cells treated with 20 % DMSO. (n = 3, mean ± SEM).

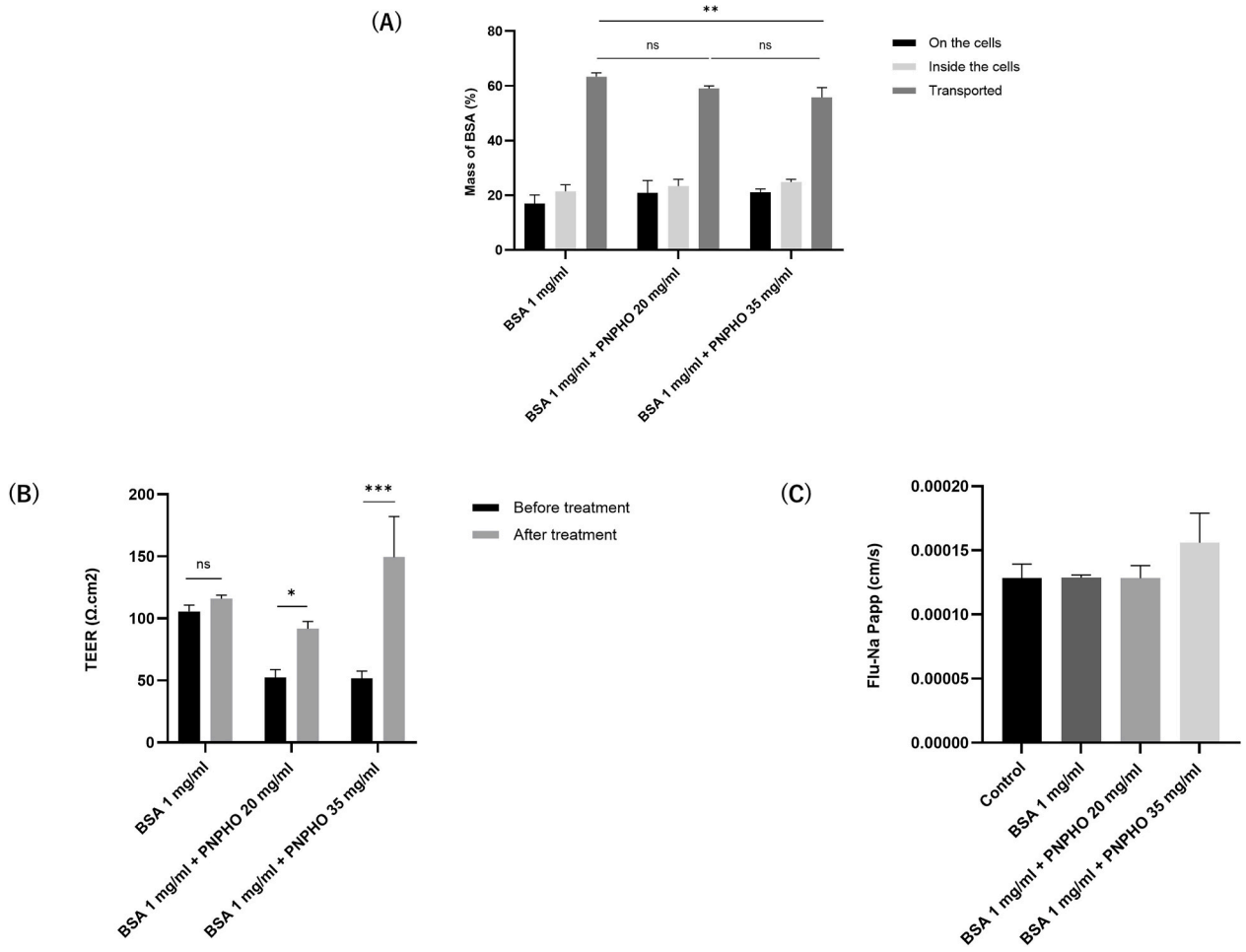

Fig. 10. Drug transport study and assessment of the epithelial barrier integrity in ALI cultured RPMI 2650 cells. (A) Transport study with BSA and BSA-PNPHO NPs formulations in RPMI 2650 cells over 4 h period. The bars represent the percentage of the total mass of BSA remaining on the apical chamber (black bars), inside the cells (light grey bars), and transported across the cells (dark grey bars), (B) TEER before and after 4 h of drug deposition on RPMI 2650 cells (C) Flu-Na Papp for the untreated cells (control) and cells treated with BSA and NPs formulations. [(n = 3, mean ± SEM), * p-value <0.05, ** p-value <0.01, *** p-value <0.001, ns, no statistical significance.

transported across the nasal cells to the basolateral chamber after 4 h of aerosol deposition for all the treatments (BSA alone and in combination with the polymer). The amount of drug retained on the apical surface of the cells and inside the cells was similar for all the treatments and was found to be significantly lower than the amount of drug transported (Fig. 10A). While no significant difference in drug permeation was observed between the free drug (63.37 ± 0.80 %) and the NPs formulation with lower polymer concentration (59.02 ± 0.55 %), BSA 1 mg/mL + PNPHO 35 mg/mL displayed a statistically significant decrease in drug transport ($p < 0.01$), *i.e.*, 55.77 ± 2.09 %, compared to the free drug *i.e.*, 63.37 ± 1.13 % at 4 h. This suggests that the polymer may provide a sustained drug release effect at higher concentrations.

To assess the barrier integrity of the RPMI 2650 ALI cultures post 4 h of treatment, TEER measurements and Flu-Na study were performed. As presented in Fig. 10B, the TEER of RPMI 2650 cells remained unaffected after exposure to BSA (before treatment: 105.51 ± 3.67 Ω cm^2 vs after treatment: 115.97 ± 1.98 Ω cm^2) for 4 h. Conversely, a significant increase in TEER value was observed for low polymer formulation (52.40 ± 4.52 Ω cm^2 (pre-treatment) to 91.81 ± 4.10 Ω cm^2 (post treatment), $p < 0.05$) and also for high polymer formulation (51.56 ± 4.23 Ω cm^2 (pre-treatment) to 149.44 ± 23.02 Ω cm^2 (post treatment), $p < 0.001$) (Fig. 10B). These findings suggest that exposure of the nasal cells to the formulations with polymer affected their barrier integrity by tightening the tight junctions, with more pronounced effect observed with the higher polymer concentration, thus, enhancing drug retention *in situ*.

To investigate the impact of all the three treatments on the paracellular permeability of nasal cells, which also depends on the integrity of the epithelial tight junctions, Papp of the paracellular marker, Flu-Na, was assessed. As shown in Fig. 10C, exposure of RPMI 2650 cells to BSA only and the formulations had no significant effect on the permeation of Flu-Na compared to the cells with no treatment (control) after 4 h of drug deposition, with Papp of 12.9 ± 7.60 × 10^{-6} cm/s, 12.8 ± 1.40 × 10^{-6} cm/s, 15.6 ± 6.92 × 10^{-6} cm/s, and 12.8 ± 1.62 × 10^{-5} cm/s, respectively. These results suggest that although, TEER values increased with increase in polymer concentration, however, the PNPHO containing NP formulations does not affect paracellular permeability, thus maintaining the epithelial barrier integrity.

Importantly, the formulation with higher polymer concentration - PNPHO 35 mg/mL exhibits significantly higher TEER and demonstrates notably less BSA transport compared to free BSA, suggesting the potential of the formulation to retain the drug for longer on the nasal surface by delaying the drug release compared to the free drug, resulting in a sustained release effect that is desirable for nasal formulations.

3.6. Drug release kinetics study

The release kinetics of BSA from NPs formulations were investigated by fitting the drug transport data to zero order, first order, Higuchi, and Korsmeyer-Peppas models (Fig. 11). The model that best described release behaviour and underlying mechanism was determined based on the correlation coefficient (R^2) and n values for each formulation summarized in Table 4. The Korsmeyer-Peppas model provided the best fit to the drug release data, as evidenced by the highest R^2 values. The n values ≤ 0.21 for both formulations, indicated that the release mechanism followed Fickian diffusion, suggesting that drug release was primarily governed by diffusion through the hydrated polymer matrix rather than matrix erosion. Since the transport study was conducted over a 4-h period, which is short relative to the expected biodegradation rate of the PNPHO polymer, polymer erosion is unlikely to significantly contribute to the drug release observed during this study duration, further supporting the predominance of diffusion as the release mechanism. Additionally, at higher polymer concentration, the NPs matrix becomes more compact and crosslinked, likely reducing pore size and increasing diffusional resistance, thereby resulting in slower drug release. The thermoresponsive behaviour of the polymer may also promote matrix densification at physiological temperature, further retarding drug diffusion and prolonging residence time in the nasal mucosa. Such a diffusion-controlled release profile is particularly beneficial for protein therapeutics, which are susceptible to enzymatic degradation in the nasal environment and require protection during epithelial transport.

A number of stimuli-responsive polymers have been already explored in several studies for PPD delivery, however, the PNPHO polymer offers potential advantages that could complement existing systems. For instance, chitosan, a natural polymer derived from crustacean chitin, exhibits considerable immunostimulatory activity [65]. In

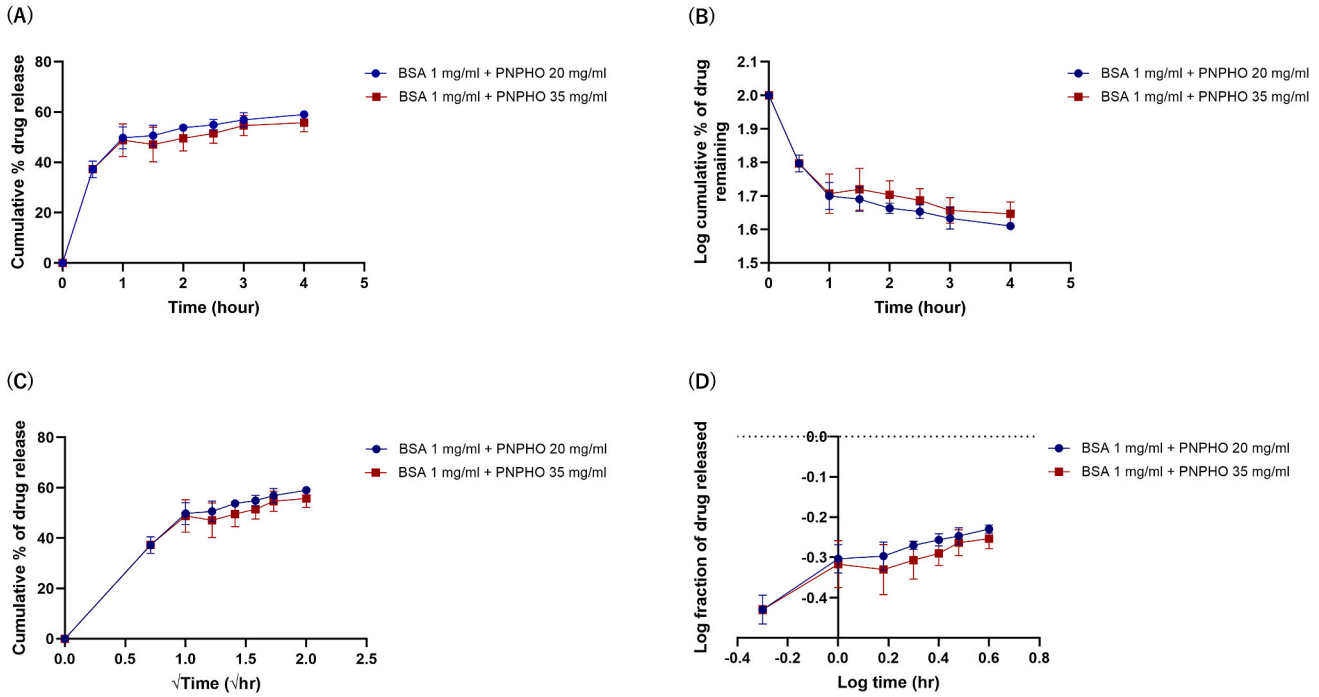

Fig. 11. Drug release kinetics plot. (A) Zero order (B) First order (C) Higuchi (D) Korsmeyer-Peppas model.

Table 4
Interpretation of parameters from drug release kinetics models for NPs formulations.

	Zero order		First order		Higuchi		Korsmeyer-Peppas		
	R^2	k_0	R^2	k_1	R^2	K_H	R^2	K_{KP}	n
BSA 1 mg/mL + PNPHO 20 mg/mL	0.59	11.18	0.68	0.18	0.85	28.27	0.91	0.46	0.21
BSA 1 mg/mL + PNPHO 35 mg/mL	0.56	10.28	0.65	0.16	0.83	26.21	0.89	0.44	0.18

contrast, the PNPHO polymer is synthetic, non-toxic, and has been shown to induce minimal inflammatory responses in multiple *in vitro* studies [26]. PLGA, while commonly used, is not inherently mucoadhesive and typically requires modification with other materials like chitosan to achieve mucoadhesion [66,67]. Similarly, PEGylated systems are generally not mucoadhesive [68,69]. In contrast, the PNPHO polymer is naturally mucoadhesive, forming a gel at physiological temperature, as demonstrated by *in vitro* mucin-binding study. Additionally, while other polymeric nanocarriers, such as poloxamer, are not biodegradable [70], the PNPHO polymer is [25,26]. Altogether, the findings of this study highlight the potential of the PNPHO polymer in enabling more efficient and targeted IN delivery of peptides and proteins, offering a promising strategy to improve current therapeutic approaches.

4. Conclusions

PPDs play a crucial role in pharmaceutical formulations due to their specificity and biocompatibility, for a wide range of chronic and acute conditions. To avoid the conventional invasive method of PPD administration, PPDs could be delivered via the IN route. However, there are significant challenges associated with IN delivery owing to the small nasal cavity area resulting in limited absorption capacity, rapid mucociliary clearance and enzymatic degradation. In the present study, a polymer-based nanocarrier system, PNPHO polymer, known for its *in-situ* gelling property at physiological temperature has been utilised to address these challenges and prolong drug residence time for enhanced absorption. PNPHO formulation at a concentration of 35 mg/mL demonstrated greater targeted deposition of BSA protein across the nasal cavity and the olfactory region compared to PNPHO 20 mg/mL and free BSA. Importantly, the 35 mg/mL PNPHO formulation exhibited lower drug transport and higher TEER values post 4 h of exposure in nasal epithelial cells, thus indicating enhanced mucoadhesion and prolonged drug release while reducing mucociliary clearance and increasing nasal surface contact time. Although, both PNPHO formulations demonstrated high encapsulation efficiency, highlighting their ability to protect peptides and proteins against biological barriers, the higher concentration of PNPHO formulation was found to be the optimum NPs formulation for increasing drug residence time and attain the desired sustained release effect. Overall, the study has shown that PNPHO polymer holds significant potential as a carrier for targeted delivery of peptide/protein using the IN route.

CRediT authorship contribution statement

Tanisha Tabassum Sayka Khan: Writing – review & editing, Writing – original draft, Visualization, Validation, Methodology, Investigation, Formal analysis, Data curation, Conceptualization. **Zara Sheikh:** Writing – review & editing, Visualization, Formal analysis, Conceptualization. **Ali Fathi:** Writing – review & editing, Visualization, Supervision, Resources, Methodology, Funding acquisition, Conceptualization. **Simin Maleknia:** Writing – review & editing, Visualization, Resources. **Farshad Oveissi:** Writing – review & editing, Visualization, Resources. **Terence Abrams:** Writing – review & editing, Visualization, Resources. **Will Knox:** Writing – review & editing, Visualization, Resources. **Luca Casettari:** Writing – review & editing, Visualization, Resources. **Mattia Tiboni:** Writing – review & editing, Visualization, Resources. **Julie Suman:** Writing – review & editing, Visualization, Resources. **Hui Xin Ong:** Writing – review & editing, Visualization, Supervision, Methodology, Funding acquisition, Conceptualization. **Daniela Traini:** Writing – review & editing, Visualization, Supervision, Methodology, Funding acquisition, Conceptualization.

Reviewer disclosures

Peer reviewers on this manuscript have no relevant financial or other relationships to disclose.

List of Abbreviations

AINI	Alberta idealized nasal inlet
ALI	Air-liquid interface
ANOVA	Analysis of variance
BBB	Blood-brain barrier
BDNF	Brain-derived neurotrophic factor
bFGF	Basic fibroblast growth factor
BSA	Bovine serum albumin
CNS	Central nervous system
DLS	Dynamic light scattering
EE	Encapsulation efficiency
EPO	Erythropoietin
FBS	Foetal bovine serum
FDA	Food and Drug Administration
Flu-Na	Fluorescein sodium
GDNF	Glial-derived neurotrophic factor
GIT	Gastrointestinal tract
GLP-1	Glucagon-like peptide-1
GLP-2	Glucagon-like peptide-2
HBSS	Hanks' balanced salt solution
hGH	Human growth hormone
hNGF	Human nerve growth factor
HPLC	High performance liquid chromatography
IGF-1	Insulin-like growth factor-1
IN	Intranasal
ITC	Isothermal titration calorimetry
MEM	Minimum essential medium
MWCO	Molecular weight cut-off
N2B	Nose-to-brain
NGI	Next generation impactor
NMR	Nuclear magnetic resonance
NPs	Nanoparticles
OB	Olfactory bulb
P_{app}	Apparent permeability coefficient
PBS	Phosphate-buffered saline
PDI	Polydispersity index
PES	Polyethersulfone
PLA	Poly (lactic acid)
PLGA	Poly (lactic-co-glycolic acid)
PNPHO	Poly(NIPAAm-co-(N-acryloxysuccinimide)-co-(polylactide/-hydroxy methacrylate)-co-(oligo (ethylene glycol)
PPDs	Peptide or protein-based drugs
PTFE	Polytetrafluoroethylene
PTH	Parathyroid hormone
RH	Relative humidity
SEM	Standard error of the mean
TEER	Transepithelial electrical resistance
TFA	Trifluoroacetic acid
TFR	Total flow rate
ζ-potential	Zeta potential

Sources of funding

Tanisha Tabassum Sayka Khan is a recipient of the International Macquarie University Research Excellence Scholarship (iMQRES) supported by New South Wales Ministry of Health and Medical Research.

This work has been partially funded by the European Union – NextGenerationEU - under the Italian Ministry of University and Research (MUR) National Innovation Ecosystem grant ECS00000041 – VITALITY - CUP [H33C22000430006].

Declaration of competing interest

The authors declare that they have no known competing financial interests or personal relationships that could have appeared to influence the work reported in this paper.

Acknowledgements

Daniela Traini is funded by a Fellowship grant from the National Health and Medical Research Council (NHMRC) of Australia (APP173363).

The authors would like to acknowledge the NCRIS-enabled Australian Proteome Analysis Facility (APAF) infrastructure at Macquarie University for providing access to its instrumentation and staff.

Data availability

Data will be made available on request.

References

[1] G. Chen, W. Kang, W. Li, S. Chen, Y. Gao, Oral delivery of protein and peptide drugs: from non-specific formulation approaches to intestinal cell targeting strategies, Theranostics 12 (3) (2022) 1419–1439, https://doi.org/10.7150/thno.61747.

[2] J. Wu, J.K. Sahoo, Y. Li, Q. Xu, D.L. Kaplan, Challenges in delivering therapeutic peptides and proteins: a silk-based solution, J. Contr. Release 345 (2022) 176–189, https://doi.org/10.1016/j.jconrel.2022.02.011.

[3] W. Al Bakri, M.D. Donovan, M. Cueto, Y. Wu, C. Orekie, Z. Yang, Overview of intranasally delivered peptides: key considerations for pharmaceutical development, Expet Opin. Drug Deliv. 15 (10) (2018) 991–1005, https://doi.org/10.1080/17425247.2018.1517742.

[4] M.L. Formica, D.A. Real, M.L. Picchio, E. Catlin, R.F. Donnelly, A.J. Paredes, On a highway to the brain: a review on nose-to-brain drug delivery using nanoparticles, Appl. Mater. Today 29 (2022), https://doi.org/10.1016/j.apmt.2022.101631.

[5] M. Bhanderi, J. Shah, B. Gorain, A.B. Nair, S. Jacob, S.M.B. Asdaq, S. Fattepur, A. S. Alamri, W.F. Alsanie, M. Alhomrani, S. Nagaraja, M.K. Anwer, Optimized rivastigmine nanoparticles coated with Eudragit for intranasal application to brain delivery: evaluation and nasal ciliotoxicity studies, Materials (Basel) 14 (21) (2021), https://doi.org/10.3390/ma14216291.

[6] L.A. Keller, O. Merkel, A. Popp, Intranasal drug delivery: opportunities and toxicologic challenges during drug development, Drug Deliv.Transl. Res. 12 (4) (2022) 735–757, https://doi.org/10.1007/s13346-020-00891-5.

[7] C.Y.J. Wong, A. Baldelli, C.M. Hoyos, O. Tietz, H.X. Ong, D. Traini, Insulin delivery to the brain via the Nasal route: unraveling the potential for Alzheimer's disease therapy, Drug Deliv.Transl. Res. 14 (7) (2024) 1776–1793, https://doi.org/10.1007/s13346-024-01558-1.

[8] M. Bose, G. Farias Quipildor, M.E. Ehrlich, S.R. Salton, Intranasal peptide therapeutics: a promising avenue for overcoming the challenges of traditional CNS drug development, Cells 11 (22) (2022), https://doi.org/10.3390/cells11223629.

[9] D. Luo, X. Ni, H. Yang, L. Feng, Z. Chen, L. Bai, A comprehensive review of advanced nasal delivery: specially insulin and calcitonin, Eur. J. Pharmaceut. Sci. 192 (2024) 106630, https://doi.org/10.1016/j.ejps.2023.106630.

[10] C. Zuglianello, E. Lemos-Senna, The nanotechnological approach for nasal delivery of peptide drugs: a comprehensive review, J. Microencapsul. 39 (2) (2022) 156–175, https://doi.org/10.1080/02652048.2022.2051626.

[11] A. Fallacara, L. Busato, M. Pozzoli, M. Ghadiri, H.X. Ong, P.M. Young, S. Manfredini, D. Traini, In vitro characterization of physico-chemical properties, cytotoxicity, bioactivity of urea-crosslinked hyaluronic acid and sodium ascorbyl phosphate nasal powder formulation, Int. J. Pharm. 558 (2019) 341–350, https://doi.org/10.1016/j.ijpharm.2019.01.012.

[12] H. Goel, V. Kalra, S.K. Verma, S.K. Dubey, A.K. Tiwary, Convolutions in the rendition of nose to brain therapeutics from bench to bedside: Feats & fallacies, J. Contr. Release 341 (2022) 782–811, https://doi.org/10.1016/j.jconrel.2021.12.009.

[13] T. Jamshidnejad-Tosaramandani, S. Kashanian, I. Karimi, H.B. Schioth, Synthesis of a rivastigmine and insulin combinational mucoadhesive nanoparticle for intranasal delivery, Polymers (Basel) 16 (4) (2024), https://doi.org/10.3390/polym16040510.

[14] T.T.S. Khan, Z. Sheikh, S. Maleknia, F. Oveissi, A. Fathi, T. Abrams, H.X. Ong, D. Traini, Intranasal delivery of glucagon-like peptide-1 to the brain for obesity treatment: opportunities and challenges, Expet Opin. Drug Deliv. 21 (7) (2024) 1081–1101, https://doi.org/10.1080/17425247.2024.2387110.

[15] A. Lofts, F. Abu-Hijleh, N. Rigg, R.K. Mishra, T. Hoare, Using the intranasal route to administer drugs to treat neurological and psychiatric illnesses: Rationale, successes, and future needs, CNS Drugs 36 (7) (2022) 739–770, https://doi.org/10.1007/s40263-022-00930-4.

[16] J. Maeng, K. Lee, Systemic and brain delivery of antidiabetic peptides through nasal administration using cell-penetrating peptides, Front. Pharmacol. 13 (2022) 1068495, https://doi.org/10.3389/fphar.2022.1068495.

[17] E.S. Fung, J.A. Parker, A.M. Powell, A. Maier, Estimating inhalation bioavailability for peptides and proteins 1 to 10 kDa in size, Regul. Toxicol. Pharmacol. 137 (2023) 105314, https://doi.org/10.1016/j.yrtph.2022.105314.

[18] H. Ueno, M. Mizuta, T. Shiiya, W. Tsuchimochi, K. Noma, N. Nakashima, M. Fujihara, M. Nakazato, Exploratory trial of intranasal administration of glucagon-like peptide-1 in Japanese patients with type 2 diabetes, Diabetes Care 37 (7) (2014) 2024–2027, https://doi.org/10.2337/dc13-0690.

[19] M. Rabiei, S. Kashanian, S.S. Samavati, H. Derakhshankhah, S. Jamasb, S.J. P. McInnes, Nanotechnology application in drug delivery to osteoarthritis (OA), rheumatoid arthritis (RA), and osteoporosis (OSP), J. Drug Deliv. Sci. Technol. 61 (2021), https://doi.org/10.1016/j.jddst.2020.102011.

[20] M. Ghaderpour, S. Kashanian, M. Nazari, M. Motiei, S. Sajadimajd, Targeted delivery of letrozole using a modified metal–organic framework as a promising candidate in breast cancer therapy, BioNanoScience 14 (3) (2024) 2872–2885, https://doi.org/10.1007/s12668-024-01408-x.

[21] S. Md, G. Mustafa, S. Baboota, J. Ali, Nanoneurotherapeutics approach intended for direct nose to brain delivery, Drug Dev. Ind. Pharm. 41 (12) (2015) 1922–1934, https://doi.org/10.3109/03639045.2015.1052081.

[22] E.J. Patharapankal, A.L. Ajiboye, C. Mattern, V. Trivedi, Nose-to-Brain (N2B) delivery: an alternative route for the delivery of biologics in the management and treatment of central nervous system disorders, Pharmaceutics 16 (1) (2023), https://doi.org/10.3390/pharmaceutics16010066.

[23] A. Sonwani, A. Pathak, K. Jain, Nanocarriers-mediated nose-to-brain drug delivery: a novel approach for the management of Alzheimer's disease, J. Drug Deliv. Sci. Technol. 98 (2024), https://doi.org/10.1016/j.jddst.2024.105855.

[24] D. Calder, A. Fathi, F. Oveissi, S. Maleknia, T. Abrams, Y. Wang, J. Maitz, K.H. Tsai, P. Maitz, W. Chrzanowski, I. Canoy, V.A. Menon, K. Lee, B.J. Ahern, N.E. Lean, D. M. Silva, P.M. Young, D. Traini, H.X. Ong, R.S. Mahmoud, H. Montazerian, A. Khademhosseini, F. Dehghani, Thermoresponsive and injectable hydrogel for tissue agnostic regeneration, Adv. Healthcare Mater. 11 (23) (2022) e2201714, https://doi.org/10.1002/adhm.202201714.

[25] A. Fathi, S.M. Mithieux, H. Wei, W. Chrzanowski, P. Valtchev, A.S. Weiss, F. Dehghani, Elastin based cell-laden injectable hydrogels with tunable gelation, mechanical and biodegradation properties, Biomaterials 35 (21) (2014) 5425–5435, https://doi.org/10.1016/j.biomaterials.2014.03.026.

[26] H. Gholizadeh, E. Landh, D.M. Silva, A. Granata, D. Traini, P. Young, A. Fathi, S. Maleknia, T. Abrams, F. Dehghani, H. Xin Ong, In vitro and in vivo applications of a universal and synthetic thermo-responsive drug delivery hydrogel platform, Int. J. Pharm. 635 (2023) 122777, https://doi.org/10.1016/j.ijpharm.2023.122777.

[27] Q. Huang, X. Chen, S. Yu, G. Gong, H. Shu, Research progress in brain-targeted nasal drug delivery, Front. Aging Neurosci. 15 (2023) 1341295, https://doi.org/10.3389/fnagi.2023.1341295.

[28] M. Gaur, S. Maurya, M.S. Akhtar, A.B. Yadav, Synthesis and evaluation of BSA-loaded PLGA-Chitosan composite nanoparticles for the protein-based drug delivery system, ACS Omega 8 (21) (2023) 18751–18759, https://doi.org/10.1021/acsomega.3c00738.

[29] P. Yadav, A.B. Yadav, Preparation and characterization of BSA as a model protein loaded chitosan nanoparticles for the development of protein-/peptide-based drug delivery system, Future J. Pharmaceut. Sci. 7 (1) (2021), https://doi.org/10.1186/s43094-021-00345-w.

[30] M. Tiboni, M. Tiboni, A. Pierro, M. Del Papa, S. Sparaventi, M. Cespi, L. Casettari, Microfluidics for nanomedicines manufacturing: an affordable and low-cost 3D printing approach, Int. J. Pharm. 599 (2021) 120464, https://doi.org/10.1016/j.ijpharm.2021.120464.

[31] K. Ozturk, M. Kaplan, S. Calis, Effects of nanoparticle size, shape, and zeta potential on drug delivery, Int. J. Pharm. 666 (2024) 124799, https://doi.org/10.1016/j.ijpharm.2024.124799.

[32] M. Danaei, M. Dehghankhold, S. Ataei, F. Hasanzadeh Davarani, R. Javanmard, A. Dokhani, S. Khorasani, M.R. Mozafari, Impact of particle size and polydispersity index on the clinical applications of lipidic nanocarrier systems, Pharmaceutics 10 (2) (2018), https://doi.org/10.3390/pharmaceutics10020057.

[33] J. Koo, C. Lim, K.T. Oh, Recent advances in intranasal administration for brain-targeting delivery: a comprehensive review of lipid-based nanoparticles and stimuli-responsive gel formulations, Int. J. Nanomed. 19 (2024) 1767–1807, https://doi.org/10.2147/IJN.S439181.

[34] T. Jamshidnejad-Tosaramandani, S. Kashanian, I. Karimi, H.B. Schioth, Synthesis of an insulin-loaded mucoadhesive nanoparticle designed for intranasal administration: focus on new diffusion media, Front. Pharmacol. 14 (2023) 1227423, https://doi.org/10.3389/fphar.2023.1227423.

[35] G. Young, N. Hundt, D. Cole, A. Fineberg, J. Andrecka, A. Tyler, A. Olerinyova, A. Ansari, E.G. Marklund, M.P. Collier, S.A. Chandler, O. Tkachenko, J. Allen, M. Crispin, N. Billington, Y. Takagi, J.R. Sellers, C. Eichmann, P. Selenko, L. Frey,

R. Riek, M.R. Galpin, W.B. Struwe, J.L.P. Benesch, P. Kukura, Quantitative mass imaging of single biological macromolecules, Science 360 (6387) (2018) 423–427, https://doi.org/10.1126/science.aar5839.
[36] G. Young, P. Kukura, Interferometric scattering microscopy, Annu. Rev. Phys. Chem. 70 (2019) 301–322, https://doi.org/10.1146/annurev-physchem-050317-021247.
[37] D. D'Angelo, S. Kooij, F. Verhoeven, F. Sonvico, C. van Rijn, Fluorescence-enabled evaluation of nasal tract deposition and coverage of pharmaceutical formulations in a silicone nasal cast using an innovative spray device, J. Adv. Res. 44 (2023) 227–232, https://doi.org/10.1016/j.jare.2022.04.011.
[38] P. Henriques, J. Bicker, A. Carona, M. Miranda, C. Vitorino, S. Doktorovová, A. Fortuna, Amorphous nasal powder advanced performance: in vitro/ex vivo studies and correlation with in vivo pharmacokinetics, J. Pharmaceut. Invest. 53 (5) (2023) 723–742, https://doi.org/10.1007/s40005-023-00630-1.
[39] M. Pozzoli, H.X. Ong, L. Morgan, M. Sukkar, D. Traini, P.M. Young, F. Sonvico, Application of RPMI 2650 nasal cell model to a 3D printed apparatus for the testing of drug deposition and permeation of nasal products, Eur. J. Pharm. Biopharm. 107 (2016) 223–233, https://doi.org/10.1016/j.ejpb.2016.07.010.
[40] Y. Zhang, C.Y.J. Wong, H. Gholizadeh, A. Aluigi, M. Tiboni, L. Casettari, P. Young, D. Traini, M. Li, S. Cheng, H.X. Ong, Microfluidics assembly of inhalable liposomal ciprofloxacin characterised by an innovative in vitro pulmonary model, Int. J. Pharm. 635 (2023) 122667, https://doi.org/10.1016/j.ijpharm.2023.122667.
[41] A. Baldelli, C. Wong, H. Oguzlu, H. Mahvizani, H.X. Ong, A.P. Rodriguez, G. Singhera, A. Thamboo, A. Singh, D. Traini, A. Pratap-Singh, Impact of amino acids on the properties of nasal dry powders, J. Drug Deliv. Sci. Technol. 87 (2023), https://doi.org/10.1016/j.jddst.2023.104848.
[42] S. Bohrey, V. Chourasiya, A. Pandey, Polymeric nanoparticles containing diazepam: preparation, optimization, characterization, in-vitro drug release and release kinetic study, Nano Converg. 3 (1) (2016) 3, https://doi.org/10.1186/s40580-016-0061-2.
[43] W. Cho, M.S. Kim, M.S. Jung, J. Park, K.H. Cha, J.S. Kim, H.J. Park, A. Alhalaweh, S.P. Velaga, S.J. Hwang, Design of salmon calcitonin particles for nasal delivery using spray-drying and novel supercritical fluid-assisted spray-drying processes, Int. J. Pharm. 478 (1) (2015) 288–296, https://doi.org/10.1016/j.ijpharm.2014.11.051.
[44] J.K. Patra, G. Das, L.F. Fraceto, E.V.R. Campos, M.D.P. Rodriguez-Torres, L. S. Acosta-Torres, L.A. Diaz-Torres, R. Grillo, M.K. Swamy, S. Sharma, S. Habtemariam, H.S. Shin, Nano based drug delivery systems: recent developments and future prospects, J. Nanobiotechnol. 16 (1) (2018) 71, https://doi.org/10.1186/s12951-018-0392-8.
[45] M. Agrawal, S. Saraf, S. Saraf, S.K. Dubey, A. Puri, U. Gupta, P. Kesharwani, V. Ravichandiran, P. Kumar, V.G.M. Naidu, U.S. Murty, Ajazuddin, A. Alexander, Stimuli-responsive in situ gelling system for nose-to-brain drug delivery, J. Contr. Release 327 (2020) 235–265, https://doi.org/10.1016/j.jconrel.2020.07.044.
[46] E. Ahmad, Y. Feng, J. Qi, W. Fan, Y. Ma, H. He, F. Xia, X. Dong, W. Zhao, Y. Lu, W. Wu, Evidence of nose-to-brain delivery of nanoemulsions: cargoes but not vehicles, Nanoscale 9 (3) (2017) 1174–1183, https://doi.org/10.1039/c6nr07581a.
[47] C.P. Costa, J.N. Moreira, J.M. Sousa Lobo, A.C. Silva, Intranasal delivery of nanostructured lipid carriers, solid lipid nanoparticles and nanoemulsions: a current overview of in vivo studies, Acta Pharm. Sin. B 11 (4) (2021) 925–940, https://doi.org/10.1016/j.apsb.2021.02.012.
[48] T.T. Nguyen, T.T.D. Nguyen, N.-M.-A. Tran, G. Van Vo, Lipid-based nanocarriers via nose-to-brain pathway for central nervous system disorders, Neurochem. Res. 47 (3) (2021) 552–573, https://doi.org/10.1007/s11064-021-03488-7.
[49] R. Boyuklieva, B. Pilicheva, Micro- and nanosized carriers for nose-to-brain drug delivery in neurodegenerative disorders, Biomedicines 10 (7) (2022), https://doi.org/10.3390/biomedicines10071706.
[50] F. Sonvico, A. Clementino, F. Buttini, G. Colombo, S. Pescina, S. Staniscuaski Guterres, A. Raffin Pohlmann, S. Nicoli, Surface-modified nanocarriers for nose-to-brain delivery: from bioadhesion to targeting, Pharmaceutics 10 (1) (2018), https://doi.org/10.3390/pharmaceutics10010034.
[51] C.Y.J. Wong, A. Baldelli, H. Gholizadeh, H. Oguzlu, Y. Guo, H. Xin Ong, A. P. Rodriguez, G. Singhera, A. Thamboo, A. Singh, A. Pratap-Singh, D. Traini, Engineered dry powders for the nose-to-brain delivery of transforming growth factor-beta, Eur. J. Pharm. Biopharm. 189 (2023) 202–211, https://doi.org/10.1016/j.ejpb.2023.06.015.
[52] M. Haim Zada, Y. Rottenberg, A.J. Domb, Peptide loaded polymeric nanoparticles by non-aqueous nanoprecipitation, J. Colloid Interface Sci. 622 (2022) 904–913, https://doi.org/10.1016/j.jcis.2022.05.007.
[53] C.Y. Wong, H. Al-Salami, C.R. Dass, Formulation and characterisation of insulin-loaded chitosan nanoparticles capable of inducing glucose uptake in skeletal muscle cells in vitro, J. Drug Deliv. Sci. Technol. 57 (2020), https://doi.org/10.1016/j.jddst.2020.101738.
[54] M. Sakhi, A. Khan, I. Khan, S. Ahmad Khan, S. Irum Khan, M. Ali Khattak, M. N. Uddin, M. Kazi, F. Nasir, Effect of polymeric stabilizers on the size and stability of PLGA paclitaxel nanoparticles, Saudi Pharm. J. 31 (9) (2023), https://doi.org/10.1016/j.jsps.2023.101697.
[55] J. Chen, W.H. Finlay, R. Vehring, A.R. Martin, Characterizing regional drug delivery within the nasal airways, Expet Opin. Drug Deliv. 21 (4) (2024) 537–551, https://doi.org/10.1080/17425247.2024.2336494.
[56] K. Inthavong, M.C. Fung, W. Yang, J. Tu, Measurements of droplet size distribution and analysis of nasal spray atomization from different actuation pressure, J. Aerosol Med. Pulm. Drug Deliv. 28 (1) (2015) 59–67, https://doi.org/10.1089/jamp.2013.1093.
[57] S. Trows, K. Wuchner, R. Spycher, H. Steckel, Analytical challenges and regulatory requirements for nasal drug products in Europe and the u.s, Pharmaceutics 6 (2) (2014) 195–219, https://doi.org/10.3390/pharmaceutics6020195.
[58] M. Gao, X. Shen, S. Mao, Factors influencing drug deposition in the nasal cavity upon delivery via nasal sprays, J. Pharmaceut. Invest. 50 (3) (2020) 251–259, https://doi.org/10.1007/s40005-020-00482-z.
[59] L. Salade, N. Wauthoz, J. Goole, K. Amighi, How to characterize a nasal product. The state of the art of in vitro and ex vivo specific methods, Int. J. Pharm. 561 (2019) 47–65, https://doi.org/10.1016/j.ijpharm.2019.02.026.
[60] M.W. Tm, W.M. Lau, V.V. Khutoryanskiy, Chitosan and its derivatives for application in mucoadhesive drug delivery systems, Polymers (Basel) 10 (3) (2018), https://doi.org/10.3390/polym10030267.
[61] S. Bhattacharjee, E. Mahon, S.M. Harrison, J. McGetrick, M. Muniyappa, S. D. Carrington, D.J. Brayden, Nanoparticle passage through porcine jejunal mucus: microfluidics and rheology, Nanomedicine 13 (3) (2017) 863–873, https://doi.org/10.1016/j.nano.2016.11.017.
[62] T.P. Crowe, W.H. Hsu, Evaluation of recent intranasal drug delivery systems to the central nervous system, Pharmaceutics 14 (3) (2022), https://doi.org/10.3390/pharmaceutics14030629.
[63] C. Rigaut, L. Deruyver, M. Niesen, M. Vander Ghinst, J. Goole, P. Lambert, B. Haut, What are the key anatomical features for the success of nose-to-brain delivery? A study of powder deposition in 3D-Printed nasal casts, Pharmaceutics 15 (12) (2023), https://doi.org/10.3390/pharmaceutics15122661.
[64] G. Williams, J.D. Suman, In vitro anatomical models for nasal drug delivery, Pharmaceutics 14 (7) (2022), https://doi.org/10.3390/pharmaceutics14071353.
[65] D. Fong, C.D. Hoemann, Chitosan immunomodulatory properties: perspectives on the impact of structural properties and dosage, Future Sci OA 4 (1) (2018) FSO225, https://doi.org/10.4155/fsoa-2017-0064.
[66] M.J. Ramalho, E. Serra, J. Lima, J.A. Loureiro, M.C. Pereira, Chitosan-PLGA mucoadhesive nanoparticles for gemcitabine repurposing for glioblastoma therapy, Eur. J. Pharm. Biopharm. 200 (2024) 114326, https://doi.org/10.1016/j.ejpb.2024.114326.
[67] R. Varela-Fernandez, X. Garcia-Otero, V. Diaz-Tome, U. Regueiro, M. Lopez-Lopez, M. Gonzalez-Barcia, M. Isabel Lema, F.J. Otero-Espinar, Mucoadhesive PLGA nanospheres and nanocapsules for lactoferrin controlled ocular delivery, Pharmaceutics 14 (4) (2022), https://doi.org/10.3390/pharmaceutics14040799.
[68] J.T. Huckaby, S.K. Lai, PEGylation for enhancing nanoparticle diffusion in mucus, Adv. Drug Deliv. Rev. 124 (2018) 125–139, https://doi.org/10.1016/j.addr.2017.08.010.
[69] N.N. Porfiryeva, I.I. Semina, I.A. Salakhov, R.I. Moustafine, V.V. Khutoryanskiy, Mucoadhesive and mucus-penetrating interpolyelectrolyte complexes for nose-to-brain drug delivery, Nanomedicine 37 (2021) 102432, https://doi.org/10.1016/j.nano.2021.102432.
[70] A. Fonseca-Garcia, E.J. Jimenez-Regalado, R.Y. Aguirre-Loredo, Preparation of a novel biodegradable packaging film based on corn starch-chitosan and poloxamers, Carbohydr. Polym. 251 (2021) 117009, https://doi.org/10.1016/j.carbpol.2020.117009.
[71] C.Y.J. Wong, A. Baldelli, O. Tietz, J. van der Hoven, J. Suman, H.X. Ong, D. Traini, An overview of in vitro and in vivo techniques for characterization of intranasal protein and peptide formulations for brain targeting, Int. J. Pharm. 654 (2024) 123922, https://doi.org/10.1016/j.ijpharm.2024.123922.